Protein-coding potential of RNAs measured by potentially translated island scores

Yusuke Suenaga[1,‡]*, Mamoru Kato[2,‡], Momoko Nagai[2], Kazuma Nakatani[1,3,4], Hiroyuki Kogashi[1,3], Miho Kobatake[1], Takashi Makino[5]

[1]Department of Molecular Carcinogenesis, Chiba Cancer Centre Research Institute, 666-2 Nitona, Chuo-ku, Chiba 260-8717, Japan

[2]Division of Bioinformatics, National Cancer Centre Research Institute, 5-1-1 Tsukiji, Chuo-ku, Tokyo 104-0045, Japan

[3]Department of Molecular Biology and Oncology, Chiba University School of Medicine, 666-2 Nitona, Chuo-ku, Chiba 260-8717, Japan

[4]Innovative Medicine CHIBA Doctoral WISE Program

[5]Laboratory of Evolutionary Genomics, Graduate School of Life Sciences, Tohoku University, Aobayama Campus 6-3, Aramaki Aza-Aoba, Aoba-ku, Sendai 980-8578, Japan

[‡]These authors equally contributed to this work

***Correspondence to:**

Yusuke Suenaga

E-mail: ysuenaga@chiba-cc.jp

Abstract

Recent studies have identified numerous RNAs that are functionally both coding and noncoding. However, the sequence characteristics that determine bifunctionality remain largely unknown. In this study, we developed and tested a potentially translated island (PTI) score, defined as the occupancy of the longest open reading frame (ORF) among all putative ORFs. We found that this score correlated with translation, including noncoding RNAs. In bacteria and archaea, coding and noncoding transcripts had narrow distributions of high and low PTI scores, respectively, whereas those of eukaryotes showed relatively broader distributions, with considerable overlap between coding and noncoding transcripts. The extent of overlap positively and negatively correlated with the mutation rates of genomes and effective population sizes of species, respectively. These overlaps were significantly increased in threatened species. In macroevolution, the appearance of the nucleus and multicellularity seem to have influenced the overlap of PTI score distributions, so that the probability of the existence of bifunctional RNAs is increased in eukaryotes. In mammalian testes, we observed an enrichment of noncoding RNAs with high PTI scores, which are candidates for bifunctional RNAs. These results suggest that the decrease in population size and the emergence of testes in eukaryotic multicellular organisms allow for the stable existence of bifunctional RNAs, consequently increasing the probability of the birth of novel coding and non-coding RNAs.

Introduction

Recent advances in RNA sequencing technology have revealed that most of the eukaryotic genome is transcribed, primarily producing noncoding RNAs (Okazaki et al. 2002; Djebali et al. 2012; Ulitsky and Bartel 2013; Kopp et al. 2018). Noncoding RNAs that are more than 200 nucleotides in length are referred to as long noncoding RNAs (lncRNAs) and are not translated into proteins (Ulitsky and Bartel 2013; Kopp et al. 2018). LncRNAs have been reported to function in multiple biological phenomena, including the regulation of transcription, modulation of protein or RNA functions, and nuclear organization (Ulitsky and Bartel 2013; Kopp et al. 2018). However, paradoxically, a large fraction of lncRNAs are associated with ribosomes and are translated into peptides (Frith et al. 2006; Ingolia et al. 2011; Bazzini et al. 2014; Ingolia et al. 2014; Ruiz-Orera et al. 2014). Peptides translated from transcripts annotated as lncRNAs have been shown to have biological functions in multiple cases in eukaryotes (Li and Liu 2019; Huang et al. 2021), and some of these translations are specific to the cellular context (Dohka et al 2021). Conversely, known protein-coding genes, such as *TP53*, have second roles as functional RNAs (Candeias 2011; Kloc et al. 2011; Huang et al. 2021). The discovery of these RNAs with binary functions has blurred the distinction between coding and noncoding RNAs, so the characteristics of RNA sequences that explain the continuity between noncoding and coding transcripts remain unclear.

During evolution, new genes originate from pre-existing genes via gene duplication or from non-genic regions via the generation of new open reading frames (ORFs) (Ohno

65 1970; Chen et al. 2013; Zhang and Long 2014; McLysaght and Guerzoni 2015;
66 McLysaght and Hurst 2016; Holland et al. 2017). The latter are *de novo* genes (Begun et
67 al. 2006; Levine et al. 2006; Begun et al. 2007; Knowles and McLysagtht 2009; Li et al.
68 2009; Toll-Riera et al. 2009; Li et al. 2010), which have been shown to regulate
69 phenotypes and diseases (McLysaght and Guerzoni 2015; Chen et al. 2013; Zhang and
70 Long 2014), including brain function and carcinogenesis in humans (Li C-Y et al. 2010;
71 Suenaga et al. 2014). lncRNAs serve as sources of newly evolving *de novo* genes (Ruiz-
72 Orera et al. 2014), some of which encode proteins. In addition to ORFs exposed to
73 natural selection, neutrally evolving ORFs are also translated from lncRNAs that stably
74 express peptides (Ruiz-Orera et al. 2018), providing a foundation for the development
75 of new functional peptides/proteins. High levels of lncRNA expression (Ruiz-Orera et
76 al. 2018), hexamer frequencies of ORFs (Sun et al. 2013; Wang et al. 2013; Ruiz-Orera
77 et al. 2014), and high peptide flexibility (Wilson et al. 2017) have been proposed as
78 determinants of coding potential; however, the molecular mechanisms by which
79 lncRNAs evolve into new coding transcripts remain unclear (Van Oss and Carvunis
80 2019).
81 In this study, we sought to identify a new indicator for determining RNA protein-coding
82 potential. Within an RNA sequence, we defined sequence segments that start with AUG
83 start codons and end with UAG, UGA, or UAA stop codons as potentially translated
84 islands (PTIs). First, we defined this indicator using PTI lengths and subsequently
85 examined the associations between the indicator and protein-coding potential. We also
86 present analyses of more than 3.4 million transcripts in 100 organisms belonging to all

87 three domains of life to investigate the relationship between the PTI score and protein-
88 coding potential over evolutionary history.
89
90 **Results**
91 **Coding transcripts show higher PTI scores in humans and mice**
92 We previously identified a *de novo* gene, *NCYM*, and showed that its protein has a
93 biochemical function (Suenaga et al 2014; Suenaga et al 2020). However, *NCYM* was
94 previously registered as a non-coding RNA in the public database, and the established
95 predictor for protein-coding potential (Wang et al 2013), the coding potential
96 assessment tool (CPAT), showed a coding probability of NCYM of 0.022, labeling it as
97 a noncoding RNA (Supplementary Figure 1). Therefore, we sought to identify a new
98 indicator for coding potential, comparing *NCYM* with a small subset of coding and non-
99 coding RNAs to determine whether NCYM has sequence features that would allow it to
100 be registered as a coding transcript (data not shown). We found that predicted ORFs,
101 other than major ORFs, seem to be short in coding RNAs. In addition, it has been
102 reported that upstream ORFs inhibit the translation of major ORFs (Calvo et al 2009).
103 Therefore, we hypothesized that the predicted ORFs may reduce the translation of major
104 ORFs, thereby becoming short in the coding transcripts, including *NCYM,* during
105 evolution. The term ORF refers to an RNA sequence that is translated into an actual
106 product; however, the biological significance of non-translating, predicted ORFs has
107 been largely ignored and remains to be characterized. Therefore, we defined a PTI as an
108 RNA sequence from the start codon sequence to the end codon sequence and did not

109 assume that it would result in a translated product. Thus, PTI can be defined even in
110 genuine non-coding RNAs. The major ORFs are often the longest PTIs (hereafter,
111 primary PTIs or pPTIs) in coding transcripts. Thus, to investigate the importance of
112 pPTIs relative to other PTIs (hereafter, secondary PTIs, or sPTIs) for the evolution of
113 coding genes, we defined a PTI score as the occupancy of the pPTI length to the total
114 PTI length (Figure 1A–B) and assumed that the PTI score was high in coding
115 transcripts. To examine this hypothesis, we first calculated the PTI scores for all human
116 transcripts. We analyzed human transcripts from the National Center for Biotechnology
117 Information (NCBI) nucleotide database for coding and noncoding (RefSeq accession
118 numbers starting with NM and NR, respectively) transcripts. The data were downloaded
119 using the Table browser (https://genome.ucsc.edu/cgi-bin/hgTables) after setting the
120 track tab as "RefSeq Genes." A total of 50,052 coding (NM) and 13,550 noncoding
121 (NR) RNAs were registered in 2018 (Supplementary Table 1). To analyze putative
122 lncRNAs with protein-coding potential, we excluded small RNAs (shorter than 200 bp)
123 or RNAs with a short pPTI (shorter than 20 amino acids) from the NR transcripts,
124 focusing on the remaining 12,827 transcripts.
125 We analyzed the relative frequencies of NM and NR transcripts, designated as $f(x)$ and
126 $g(x)$, respectively (Figure 1C), where x indicates the PTI score. In human transcripts,
127 $g(x)$ showed a distribution that shifted to the left with an apex of 0.15; in contrast, the
128 distribution of $f(x)$ shifted to the right with an apex of 0.55 (Figure 1C, upper panel). As
129 a control, we generated nucleic acid sequences in which A/T/G/C bases were randomly
130 assigned with equal probabilities. In the controls, the relative frequencies of PTI scores

131 were shifted to the left in both coding and noncoding transcripts (Figure 1C, bottom
132 panel). The controls that randomly shuffled the original sequence without affecting the
133 number of A/T/C/G bases in each transcript also had relative frequencies of PTI scores
134 shifted to the left in both coding and noncoding transcripts (Supplementary Figure 2A).
135 Similar results were obtained using a dataset from the Ensembl database
136 (Supplementary Figure 2B). We also calculated the PTI scores of mouse transcripts
137 from RefSeq and Ensembl and found that the distribution of $f(x)$ was shifted to the right
138 with an apex of 0.55 (Supplementary Figure 2C), similar to that of human transcripts.
139 These results suggest that the sequences, not lengths, of the coding transcripts increased
140 the PTI scores in mice and humans.
141

142 **PTI scores correlate with protein-coding potential in humans and mice**

143 Next, we examined the relationship between PTI score and protein-coding potential.
144 Based on the PTI score distributions of coding and noncoding transcripts, protein-
145 coding potential $F(x)$ was defined as the probability of being a coding transcript with a
146 PTI score of x. A sample $F(0.15)$ calculation for human transcripts is shown in Figure
147 1D. This result indicates that any given human RNA transcript with a calculated PTI
148 score of 0.15 has a protein-coding potential $F(x)$ of 0.183. $F(x)$ was correlated with PTI
149 scores ≤ 0.65 (Figure 1E and Supplementary Figure 3A). The protein-coding potentials
150 of sequences in RefSeq data slightly decreased after peaking at 0.65 (Figure 1E),
151 whereas those of sequences in the Ensembl data remained high (Supplementary Figure

152 3A). The $F(x)$ of human transcripts was approximated by the following linear

153 regression:

154

155 Based on Ensembl data,

156 $F(x) = 1.301x + 0.0072$ ($x \leq 0.65$), $R^2 = 0.984$

157

158 Based on RefSeq data,

159 $F(x) = 1.313x + 0.0189$ ($x \leq 0.65$), $R^2 = 0.990$

160

161 The intercepts were near zero, and the slopes were approximately 1.3. Using these

162 formulas, we can calculate the protein-coding potential $F(x)$ for any given human

163 transcript with a PTI score of ≤ 0.65. For example, the $F(x)$ of *NCYM* was calculated to

164 be 0.746 and 0.765 based on the Ensembl and RefSeq databases, respectively

165 (Supplementary Figure 1D). In contrast, $F(x)$ for the controls was not correlated with

166 the PTI scores (Figure 1E, bottom panel, and Supplementary Figure 3A). Similar results

167 were obtained for the mouse transcripts (Supplementary Figures 3B). The $F(x)$ of the

168 mouse transcripts (PTI score ≤ 0.65) was approximated as follows:

169

170 Based on Ensembl data,

171 $F(x) = 1.142x + 0.067$, $R^2 = 0.982$

172

173 Based on RefSeq data,

174 $F(x) = 1.482x - 0.061$, $R^2 = 0.990$

175

176 For both human and mouse transcripts, the PTI score correlated linearly with the

177 protein-coding potential at PTI scores ≤ 0.65. Moreover, when the PTI score limit

178 approached 0, the probability of the transcript being a coding RNA was 0 (Figure 1E

179 and Supplementary Figure 3).

180

181 **Characterization of high-scoring human lncRNAs**

182 Next, we investigated whether the PTI score is useful for identifying coding RNAs

183 among NR transcripts. From the 7,144 transcripts registered as noncoding genes in

184 2015, we excluded small RNAs (< 200 nucleotides) and those with short primary PTIs

185 (< 20 residues). Among the remaining 6,617 NR genes, 219 were reassigned as NM

186 over the past 3 years (Supplementary Table 2), including the previously identified *de*

187 *novo* gene *MYCNOS/NCYM* (Suenaga et al. 2014). The percentage of reclassification

188 increased for NR transcripts with high PTI scores (Figure 1F). Thus, a high PTI score is

189 a useful indicator of coding transcripts. NR transcripts with high protein-coding

190 potential (0.6 ≤ PTI score < 0.8) were then extracted, and the domain structure of the

191 pPTI amino-acid sequence was assessed using BLASTP. A total of 217 transcripts

192 showed putative domain structures in pPTI, whereas 310 did not (Supplementary Table

193 3). Transcripts with domain structures are often derived from transcript variants,

194 pseudogenes, or readthrough of coding genes; those without domain structures are often

195 derived from antisense or long intergenic noncoding RNAs (lincRNAs) (Table 1).

196 We next examined the functions of genes generating NR transcripts with high coding
197 potential (0.6 ≤ PTI score < 0.8). We divided the NR transcripts into those with and
198 without putative domains to investigate novel coding gene candidates, either originating
199 from pre-existing genes or created from non-genic regions. Analysis using the Database
200 for Annotation, Visualization, and Integrated Discovery (DAVID) functional annotation
201 tool (Huang et al. 2009a, 2009b) showed that NR transcripts without domain structures
202 were derived from original genes related to transcriptional regulation, multicellular
203 organismal processes, and developmental processes (Supplementary Table 4). Among
204 the target genes of transcription factors, NMYC (MYCN), TGIF, and ZIC2 were ranked
205 in the top three and are all necessary for forebrain development (Supplementary Table
206 4) (Brown et al. 1998; Gripp et al. 2000; van Bokhoven et al. 2005). We observed that
207 NR transcripts with domain structures originating from genes that undergo alternative
208 splicing are related to organelle function and are expressed in multiple cancers,
209 including respiratory tract tumors, gastrointestinal tumors, retinoblastomas, and
210 medulloblastomas (Supplementary Table 5). Similar analyses were conducted in mice
211 (Supplementary Tables 6–8) and *C. elegans* (Supplementary Tables 9–11). In mice, the
212 original genes related to protein dimerization activity (Supplementary Table 7) and
213 nucleotide binding or organelle function (Supplementary Table 8) were enriched in
214 high-PTI score lncRNAs with and without conserved domains, respectively. In *C.*
215 *elegans*, the original genes related to embryo development (Supplementary Table 10)
216 and chromosome V or single-organism cellular processes (Supplementary Table 11)

were enriched. Therefore, the relationship between brain development and cancer in the function of high-PTI-score lncRNAs seems to be specific to humans.

PTIs affect the protein-coding potential predicted by *K*a/*K*s

To examine the relationship between PTI scores and natural selection in the prediction of protein-coding potential, we calculated the ratio of nonsynonymous (*K*a) to synonymous (*K*s) values by comparing human transcripts with syntenic genomic regions of chimpanzees and mice (Figure 1G). Transcripts were selected based on the syntenically conserved regions: 44,593 (vs. chimp) and 14,016 (vs. mouse). We found a linear relationship between the $F(x)$ and PTI scores in the conserved transcripts (Figure 1G, left panels). As predicted, coding transcripts exhibited *K*a/*K*s < 0.5 at a higher frequency than did noncoding transcripts, with large differences observed when for PTI scores > 0.9 or < 0.1, with the smallest difference for PTI scores of approximately 0.35 to 0.45 (Figure 1G, right panels). These results indicate that for transcripts with PTI scores near the highest or lowest values, the conservation of ORF/pPTI sequences (negative selection, *K*a/*K*s < 0.5) determines the coding potential. In contrast, for transcripts with PTI scores between 0.35 and 0.45, the conservation of ORF/pPTI sequences has almost no effect on the coding potential, and thus ORF/pPTI sequences have more potential to evolve neutrally. Therefore, noncoding transcripts showing both negative selection (*K*a/*K*s < 0.5) and the highest PTI scores may include new coding transcript candidates. We list 23 such transcripts in Supplementary Table 12, including

238 four transcript variants of a previously identified lncRNA that encodes a tumor-

239 suppressive small peptide, HOXB-AS3 (Huang et al 2017).

240

241 **Translation of small peptides shifts PTI score distributions**

242 To investigate the effect of translation on the PTI score, we calculated the PTI scores of

243 lincRNAs encoding small proteins and compared them with the PTI score distribution

244 of all lincRNAs (Figure 2A). We found that lincRNAs translating small proteins shifted

245 to higher PTI scores, and lincRNAs with PTI scores around 0.45 were increased

246 compared to the distribution of all lincRNAs.

247 ORF coverage, ORF size, and transcript length are indicators that have been used to

248 predict the coding potential of transcripts (Wang et al. 2013; Zeng et al 2018). We

249 calculated these three values for lincRNAs with translation products, and their

250 distribution was compared with that of all lincRNAs. The comparison revealed no

251 rightward shift in the peak, but there was a shift in the higher values of ORF coverage

252 (Supplementary Figure 4A). On the other hand, there was no rightward shift in ORF

253 size or transcript length (Supplementary Figure 4B and 4C). Therefore, the translation

254 of non-coding RNAs was strongly correlated with the PTI score, but not with transcript

255 length, ORF size, or ORF coverage.

256 Next, to examine whether PTI scores were associated with translation occupancy of

257 ORFs in coding RNAs, we defined the ORFs in which translation products were

258 identified in the sPTIs: uORFs, sPTIs with translation products detected in the 5'UTRs;

259 sORFs, PTIs with translation products detected in other frames overlapping with ORFs

260 of major proteins; and dORF, sPTIs with translation products detected in the 3'UTRs
261 (Figure 2B). When the PTI scores of coding RNAs with uORF, sORF, and dORF were
262 calculated and the PTI score distribution was compared with that of all coding RNAs,
263 the PTI scores shifted to lower values, peaking at 0.35-0.45 (Figure 2C). Although there
264 are differences in the effect of the location of the translated sPTI in a dataset from a
265 different database, the PTI score distribution remained similar, that is, it shifted to lower
266 values and increased the number of coding transcripts with PTI scores of 0.35-0.45
267 (Supplementary Figure 5). These results support the idea that the PTI score is related to
268 the occupancy of major ORFs in the translation of RNAs. In addition, when considering
269 the results in Figure 1G, translation of noncoding RNAs and sPTI in coding RNAs may
270 increase the chances of pPTI/ORF sequences evolving neutrally by increasing
271 transcripts with PTI scores of 0.35-0.45.
272
273 **Relationship between PTI score and relative frequencies of coding/noncoding**
274 **transcripts in 100 organisms**
275 To analyze the relationship between PTI scores and protein-coding potential in a broad
276 lineage of organisms, we selected 100 organisms, consisting of five bacteria, ten
277 archaea, and 85 eukaryotes (Supplementary Table 1), and calculated PTI scores for
278 more than 3.4 million transcripts (Supplementary Table 1). Phylogenetic trees of the
279 cellular organisms are presented on a logarithmic time scale, along with the number of
280 species in each lineage used in the analyses in Figure 3. To examine the evolutionary
281 conservation of the linear relationship between the PTI score and protein-coding

282 potential in humans and mice, we selected a relatively large number of mammalian
283 species (36). Species with fewer than three lncRNAs were not used to calculate $g(x)$ and
284 were not included in the histograms illustrating their relationship with the PTI score
285 (Figures 4 and 5). For all organisms, the relative frequency of coding transcripts $f(x)$
286 was shifted to the right (higher PTI score) compared to random or random shuffling
287 controls (Figures 4 and 5; Supplement Figures 6 and 7).
288 In bacteria and archaea, $f(x)$ and $g(x)$ exclusively exhibited high and low PTI scores,
289 respectively, indicating a clear boundary between coding transcripts and lncRNAs in
290 terms of PTI scores (Figure 4 and Supplementary Figure 6). In addition, the highest
291 frequency of coding transcript $f(x)$ presenting a PTI score was 0.75 in all examined
292 bacteria (Figure 4) and ≥ 0.75 in archaea (Supplementary Figure 6). Among eukaryotes,
293 unicellular organisms and non-vertebrates showed the highest frequencies of coding
294 transcripts at 0.65 or 0.75 (Figure 4), while most vertebrates showed the highest values
295 ≤ 0.65 (Figures 4 and 5). In addition, the $f(x)$ distribution in vertebrates was broad and
296 shifted to the left (lower PTI scores) relative to those of bacteria and archaea (Figure 4
297 and 5). In sharp contrast to $f(x)$, the relative frequency of lncRNAs $g(x)$ was shifted to
298 the right (higher PTI scores) in eukaryotes, including *G. lamblia,* which belongs to the
299 earliest diverging eukaryotic lineage and lacks mitochondria (Figure 4). Since the
300 distribution of $f(x)$ in the Excavata, including *G. lamblia,* showed a similar pattern to
301 that of bacteria, the right shift of $g(x)$ seems to be an earlier event than the left shift of
302 $f(x)$ in the evolution of eukaryotes. Collectively, the right and left shifts of $f(x)$ and $g(x)$

303 contribute to blurring the boundary between coding and noncoding transcripts in

304 eukaryotes.

305

306 **PTI score distribution overlap is inversely correlated with effective population size**

307 In general, eukaryotes (particularly multicellular organisms) have smaller effective

308 population sizes than prokaryotes, with higher mutation rates due to the effect of genetic

309 drift (Lynch et al 2016). We defined an indicator of coding/noncoding boundary

310 ambiguity (overlapping score, O_{pti}) and examined the relationship between O_{pti} and

311 effective population size and mutation rate, using data from a previous study (Lynch et

312 al 2016). The overlapping score based on ORF coverage, O_{cov}, was also defined for

313 comparison (Supplementary Figure 8). Of the 35 species used in this study, 11 had no

314 more than five lncRNAs with pPTIs longer than 20 residues, and transcripts of the

315 remaining 24 species (Supplementary Table 13 and Supplementary Figure 8) were used

316 for the analysis. Similar to a previous report (Lynch et al 2016), the effective population

317 size was inversely proportional to the mutation rate of genomic DNA, even in the

318 remaining 24 species (exponent = −1.126, R^2 = 0.6842, Figure 6A). O_{pti} positively and

319 negatively correlated with mutation rates and effective population size, respectively,

320 with relationships that could be approximated as logarithmic (R^2 = 0.7578) or

321 exponential functions (R^2 = 0.4667). In contrast, ORF coverage (O_{cov}) showed a weaker

322 relationship with mutation rates and effective population size (Supplementary Figure 9).

323 Substituting the maximum value of O_{pti}, 1 into this exponential approximation (Figure

324 6A, right upper panel) yields the minimum effective population size, which is 1001.28.

325 This is consistent with the observation that the minimum effective population size in
326 conservation biology is approximately 1000 (Frankham et al 2014). This result led us to
327 consider the possibility that O_{pti} might be elevated in endangered organisms. We
328 calculated O_{pti} for 35 vertebrate species on the IUCN Red List (left panel, Figure 6B;
329 Supplementary table 1), and found that species at risk of extinction had significantly
330 higher O_{pti} than species with little risk of extinction (Least Concern, LC). In addition,
331 among LCs, O_{pti} was higher for species with decreasing numbers compared to those
332 with stable populations (right panel, Figure 6B; Supplementary table 1).
333
334 **Relationship between PTI score and protein-coding potential**
335 The overlapping of relative frequencies in $f(x)$ and $g(x)$ led us to examine the
336 relationship between the PTI score and protein-coding potential $F(x)$ in eukaryotes. To
337 avoid being misled by small sample numbers, we selected 32 species with more than
338 1000 lncRNAs that contained pPTIs to calculate $F(x)$ (Figure 7 and Supplementary
339 Figure 10). In humans and mice, the relationship between the PTI score and $F(x)$ was
340 approximated with a linear function passing through the origin of the PTI score ≤ 0.65.
341 Therefore, we used linear approximation of the $F(x)$ of 32 species and found that 27 of
342 the 32 species were well approximated by linear functions (indicated as linear group, L,
343 in Figure 7 and Supplementary Figure 10). In *U. americanus*, *C. canadensis*, and *G.*
344 *gorilla*, fewer than five lncRNAs exhibited PTI scores of 0.05; thus, we eliminated the
345 $F(0.05)$ in these species for the approximation by linear function (indicated with
346 asterisks in Figure 7). The $F(x)$ of the remaining five species that showed $O_{pti} > 0.7$ did

347 not fit in linear approximations (indicated as constant group C in Figure 7) and were
348 characterized by low slope values. They belonged to plants (*Z. mays*), reptiles (*A.*
349 *carolinensis*), and mammals (*O. anatinu*, *S. boliviensis*, and *G. gorilla*) (Figure 7). In
350 these species, PTI scores showed a weaker association with protein-coding potential.
351 We noticed that these species may have small effective population sizes, possibly
352 because of the risk of extinction (*O. anatinu* and *G. gorilla*) or artificial selection as pets
353 (*A. carolinensis* and *S. boliviensis*) or as crops (*Z. mays*).
354
355 **Characteristics of RNA virus genomes in human and bacterial cells**
356 In sharp contrast to the coding transcripts of bacteria and archaea, the PTI scores of
357 coding transcripts of eukaryotes overlapped with those of noncoding RNAs due to their
358 broad distribution of low PTI scores. To investigate the molecular mechanism
359 underlying the distinct distribution of coding transcripts between bacteria and
360 eukaryotes, we analyzed the genome sequences of RNA viruses that infect human or
361 bacterial cells. Positive-sense single-stranded RNAs, or (+) ssRNAs, are parts of the
362 viral genome that generate mRNAs and are translated into viral proteins via the host
363 translation system. Therefore, efficient translation in host cells contributes to the
364 replication of (+) ssRNA viruses. We speculated that PTIs other than bona fide ORFs
365 affect the coding potential of the viral genome in host cells. Multiple bona fide ORFs
366 are present in viral genomes. Thus, we extended the concept of PTIs to multiple ORFs
367 in viral RNA genomes (Figure 8A) and set the viral ORF (vORF) score.

368 Among the positive sense ssRNA viruses registered in the NCBI database, 198 were
369 human viruses and 13 were bacteriophages. We eliminated the viruses that produced
370 viral proteins by exceptional translation mechanisms such as ribosome frameshifting,
371 alternative initiation sites, ribosome slippage, and RNA editing, focusing on the
372 remaining 95 human viruses, including nine retroviruses (Supplementary Table 14) and
373 10 bacteriophages (Supplementary Table 15). The relative frequencies of the human
374 viruses and bacteriophages showed distinct peaks at PTI scores of 0.65 and 0.75,
375 respectively (Figure 8B). These values correspond to the PTI scores of the highest
376 protein-coding potential in humans (Figure 1E and Supplementary Figure 3A) and the
377 highest frequency of coding transcripts in bacteria (Figure 4). In addition, the relative
378 frequency of human viruses showed a broader distribution of low PTI scores compared
379 to bacteriophages, particularly in human retroviruses (Figure 8B). Therefore, RNA virus
380 genomes appear to have sequence characteristics that maximize their protein-coding
381 potential in host cells.
382
383 **The relationship between PTI scores and tissue-specific expressions**
384 The right shift of the PTI score distribution for noncoding RNAs is pronounced in
385 eukaryotes, especially in multicellular organisms (Figures 4 and 5). To examine the
386 possibility that different tissues in multicellular organisms show different PTI
387 distributions for noncoding RNAs, we analyzed transcriptome data to calculate the PTI
388 scores of human noncoding transcripts expressed in multiple tissues (Figure 8C). The
389 PTI score distributions were similar for almost all tissues, but, as an exception, they

390 shifted to higher values for mature testes (Figure 8C). Similar results were also obtained
391 for opossums, rats, mice, and macaques, although their shifts were weaker than those of
392 humans (Supplementary figure 11). Furthermore, the noncoding transcripts that were
393 expressed in a tissue-specific manner had higher PTI scores than ubiquitously expressed
394 noncoding transcripts in humans (Figure 8D) and the other four species (Supplementary
395 figure 12). The relationship between the specificity of expression and the PTI score was
396 also found for human coding transcripts (Supplementary figure 13). These results
397 suggest that the tissue-/cell type-specific expression of transcripts evolved in
398 multicellular eukaryotes contributes to increased PTI scores for noncoding transcripts.
399 Since the majority of tissue-specific transcripts were expressed in matured testes (7,573
400 of 8,523 transcripts (89%) in the highest specificity group for humans), the evolution of
401 the testis also seems to contribute to the existence of high PTI score-noncoding RNAs,
402 thus contributing to the birth of new coding genes.
403
404 **Discussion**
405 Here, we showed that PTI scores are associated with protein-coding potential in cellular
406 organisms. In bacteria and archaea, the PTI-score distributions for noncoding and
407 coding transcripts were distinct (low and high scores), whereas they were merged in
408 eukaryotes.
409 Right shifts in the distribution of noncoding RNA occurred in *G. lamblia*, one of the
410 earliest diverging eukaryotes, which are binucleate and lack mitochondria, peroxisomes,
411 and a typical Golgi apparatus (Ankarklev et al. 2010; Bartelt et al. 2015; Buret et al.

412 2020) and were commonly observed in all eukaryotes examined. Moreover, functional
413 noncoding RNAs, by definition, should not be translated by ribosomes in cells.
414 However, in bacteria and archaea, newly transcribed RNAs are immediately bound by
415 ribosomes (Miller et al. 1970; French et al. 2007) and do not have the chance to escape
416 translation. Thus, as expected, transcripts with noncoding functions in bacteria and
417 archaea showed low PTI scores (top panel, Figure 9A). Alternatively, in eukaryotes, the
418 existence of the nucleus prevents the immediate binding of lncRNAs by ribosomes, so
419 cytoplasmic translocation from the nucleus is required for translation. Therefore,
420 eukaryotic lncRNAs may function in the nucleus even with high PTI scores, and the
421 subsequent evolution of cytosolic translocation of these noncoding RNAs may
422 contribute to the origination of new coding genes (middle panel, Figure 9A). Thus, the
423 pervasive transcription of the genome seems to help eukaryotes to create new functional
424 noncoding/coding RNAs, while being disadvantageous for bacteria and archaea by
425 increasing the risk of transcription of high-PTI-score transcripts, leading to immediate
426 translation of wasteful and/or toxic proteins (top and middle panels, Figure 9A,
427 Monsellier et al. 2007). In addition, multicellular organisms have a variety of
428 intracellular environments because of the large number of cell types, which may
429 increase the possibility of the existence of an intracellular environment in which newly
430 created proteins are not toxic (bottom panel, Figure 9A). Since the possibility that a new
431 protein will not be toxic in multiple intracellular environments is lower than the
432 possibility that it will not be toxic in a particular intracellular environment, noncoding

433 RNAs that are ubiquitously expressed need to have lower PTI scores than those with
434 specific expression (bottom panel, Figure 9A).
435 Kaessmann proposed an "out of the testes hypothesis," arguing that the testis facilitates
436 the birth and evolution of new genes in animals. The germ cells (spermatocytes and
437 spermatids) in the testes have an active chromatin state, and global transcription occurs,
438 increasing the possibility of generating new coding genes (Kaessmann 2010).
439 Consistent with this hypothesis, our results showed that the PTI score distribution of
440 noncoding RNAs shifted to higher values only in mature testes with spermatocytes and
441 spermatids, but not in immature testes or in other tissues. In addition, most transcripts
442 with tissue-specific expression were found in mature testes, and these noncoding RNAs
443 had high PTI scores. These results suggest that new coding genes are generated from
444 noncoding RNAs with high PTI scores that are specifically expressed in germ cells of
445 the mature testis.
446 Multiple human noncoding RNAs with high PTI scores have been reclassified as coding
447 genes over the past 3 years, including the human *de novo* gene *NCYM* (Suenaga et al.
448 2014; Suenaga et al. 2020). Because *de novo* gene products have no known domain
449 structures, high PTI score-noncoding transcripts without putative domains may be good
450 candidates as novel *de novo* genes in eukaryotes. *NCYM* is an antisense gene of *MYCN*,
451 whose protein product stabilizes the MYCN protein (Suenaga et al. 2014). MYCN
452 directly stimulates *NCYM* and *OCT4* transcription, whereas OCT4 induces MYCN
453 (Kaneko et al. 2015). This functional interplay forms a positive feedback loop, allowing
454 these genes to induce each other's expression in human neuroblastomas (Suenaga et al.

455 2014; Islam et al. 2015; Kaneko et al. 2015; Shoji et al. 2015). Functional annotation of
456 noncoding genes without putative domains was related to transcriptional regulation, and
457 the target genes of transcription factors, including MYCN, TGIF, and ZIC2, were
458 enriched. As *de novo* emergence of *NCYM* occurred in Homininae, NCYM-mediated
459 MYCN activation may modulate human *de novo* gene births during evolution,
460 regulating the transcription of *MYCN* target genes. Notably, both NCYM and MYCN
461 are expressed in germ cells of the testes (Suenaga et al 2014; Kanatsu-Shinohara et al
462 2016), and MYCN has been shown to regulate the self-renewal of spermatogonial stem
463 cells (Kanatsu-Shinohara et al 2016). Furthermore, a recent study showed that binding
464 sites for transcription factors, including MYCN, are mutational hotspots in human
465 spermatogonia (Kaiser et al. 2021). Both *TGIF* and *ZIC2* are mutated in
466 holoprosencephaly, a disorder caused by a failure in embryonic forebrain development
467 (Brown et al. 1998; Gripp et al. 2000), whereas *MYCN* mutations cause Feingold and
468 megalocephaly syndromes, which are associated with reduced and increased brain size,
469 respectively (van Bokhoven et al. 2005; Kato et al. 2019). Thus, the present study also
470 provides a list of candidate human *de novo* genes possibly involved in brain
471 development and brain-related diseases.
472 Relative frequencies of positive-sense ssRNA viruses exhibit sharp peaks at vORF
473 scores of 0.75 in bacteriophages and 0.65 in human viruses, indicating the adaptation of
474 RNA viruses to host cells by maximizing the protein-coding potential of their genomes.
475 Immediately after viral infection, the viral (+) ssRNA genomes, save for those of
476 retroviruses, are used as templates for translation in the host cytosol. Thus, the distinct

477 translation systems between humans and bacteria likely affect the left shift in the viral
478 genome peak, as well as the left shift in coding RNA distribution in eukaryotes. In
479 retroviruses, reverse transcriptase produces double-stranded DNA using the viral
480 genome as a template, which is then inserted into the host genome. The viral genome is
481 subsequently transcribed in the nucleus, and its mRNA is transported to the cytoplasm
482 where protein products are translated in a manner similar to that of host proteins.
483 Therefore, the relatively lower vORF score distribution in human retrovirus genomes is
484 likely a function by the nuclear localization of the provirus, which may promote the
485 diversification of PTI scores of RNA genomes via adaptation to host cellular
486 mechanisms other than translation, such as cytosolic translocation.
487 While the overlap of PTI score distributions of coding/noncoding transcripts seems to
488 be beneficial by facilitating new gene birth, excessive overlap in PTI score distributions
489 was found in species at the risk of extinction. Because the extent of the overlap (O_{pti})
490 positively and negatively correlates with higher mutation rates and effective population
491 sizes, respectively, the small effective population sizes in multicellular eukaryotes seem
492 to increase the overlap by accumulation of the slightly deleterious or beneficial
493 mutations driven by random drift, as predicted by neutral theory (Kimura 1968; Kimura
494 1983) and nearly neutral theory (Ohta 1992). Translation of noncoding RNA or sPTIs in
495 coding RNAs caused right and left shifts in PTI score distributions, respectively. The
496 mutations that cause these translations may be beneficial for increasing the possibility
497 of evolution of new functional RNAs or regulatory mechanisms and be deleterious for
498 inhibiting existing coding/noncoding functions. Translation of small proteins from

499 noncoding RNAs seems to inhibit the noncoding functions of RNA because of ribosome
500 binding and subsequent translation. In contrast, translation of sPTIs in coding RNAs
501 seems to inhibit translation of major ORFs because of the competition for translation
502 (Calvo et al 2009) without the evolution of specific regulatory mechanisms, such as the
503 recently discovered mechanism in dORF (Wu et al. 2021).
504 According to the drift-barrier hypothesis (Lynch et al 2010; Lynch et al 2016), the
505 performance of any molecular trait is expected to become more refined in larger
506 population sizes, because the effects of selection relative to random drift are stronger.
507 Consistent with this hypothesis, we found that the molecular traits of coding or
508 noncoding RNAs were prominent in bacteria/archaea and weak in multicellular
509 eukaryotes, allowing the existence of bifunctional RNAs. The excessive overlap of PTI
510 score distributions ($O_{pti} > 0.7$) diminished the correlation between the PTI score and
511 protein-coding potential. This indicates that both coding and noncoding transcripts lost
512 their molecular traits as coding and noncoding RNAs in terms of PTI score, which
513 became lethal or highly deleterious for the species.
514 Species with decreasing population sizes showed significantly higher O_{pti} compared
515 with species with a stable population size, even in the LC group. Combined with the
516 results discussed above, we propose a novel model of new gene origination in which
517 new gene birth occurs in response to decreased effective population sizes (Figure 9B).
518 At stable population sizes, natural selection maintains molecular traits of existing genes,
519 and thus existing coding and noncoding functions of RNA stably exist with high and
520 low PTI scores with low overlap of PTI score distribution of coding/noncoding

521 transcripts. When new environments reduce the effective population size of species, the
522 driving force of fixation/elimination of mutations changes from natural selection to
523 random drift. This increases the probability of fixation of slightly deleterious/beneficial
524 mutations, resulting in an increase in the overlap of PTI score distributions between
525 coding and noncoding transcripts. The overlap allows the existence of bifunctional
526 RNAs as candidates for new functional coding or noncoding transcripts. When the
527 effective population size approaches 1,000 because of rapid decline, the accumulation
528 of deleterious mutations decreases the long-term evolutionary potential of populations,
529 leading to extinction. On the other hand, when the speed is slow enough for beneficial
530 mutations to be fixed in the populations, the newly evolved coding/noncoding
531 transcripts contribute to an increase in the effective population size, resulting in
532 adaptation of the species to new environments. The increase in the effective population
533 size leads to an increase in the effect of natural selection on the new functions of
534 coding/noncoding genes as well as pre-existing genes. Thus, if nuclear evolution and
535 multicellularity contribute to the generation of lncRNAs with high PTI scores and
536 subsequent generation of novel coding genes (Figure 9A), the ability to generate new
537 genes in response to population decline (Figure 9B) may be greatest in eukaryotic
538 multicellular organisms.
539
540 In conclusion, the PTI score is an important indicator for integrating the concept of gene
541 birth into classical evolutionary theory, thereby contributing to the elucidation of the
542 molecular basis for the evolution of complex species, including humans. In the future, it

543 will be necessary to calculate PTI scores based on the transcriptomes of additional

544 species to test our hypothesis that positioning new gene birth as a countermeasure to the

545 decline in effective population size.

546

547 **Materials and Methods**

548 **Potentially translated islands (PTIs)**

549 ***Definition***

550 PTIs are defined as sequence segments beginning at AUG and ending with any of the

551 UAA, UAG, or UGA stop codons in the 5′ to 3′ direction within an RNA sequence in all

552 three possible reading frames (Figure 1A).

553 ***Example***

554 The PTIs in the human *de novo* gene *NCYM* (Suenaga et al. 2014) were identified using

555 the cDNA sequence (Supplementary Figure 1A) and are shown in bold characters

556 (Supplementary Figure 1B). Further information is included in the Supplementary

557 Notes.

558

559 **The length of a PTI and primary/secondary PTIs**

560 ***Definition***

561 The PTI length is defined as the length of the amino acid sequence, excluding the stop

562 codon, and is represented by l (Figure 1A). In an RNA sequence, the longest PTI is

563 designated as the primary PTI (pPTI), whereas the others are termed secondary PTIs

(sPTIs). The lengths of pPTI and sPTI are described as l_{pPTI} and l_{sPTI}, respectively (Figure 1A).

Example

The shortest possible PTI is "AUGUAA," "AUGUAG," or "AUGUGA," with a single methionine. For example, the NCYM transcript has a pPTI with a length of 109 in frame 1, three sPTIs with lengths of 69, 8, and 6, respectively, in frame 2, and no PTIs in frame 3 (Supplementary Figure 1C and D).

Characteristics

Therefore, the following relationship between the lengths of pPTI and sPTI is held:

$$1 \leq l_{\mathrm{sPTI}} \leq l_{\mathrm{pPTI}} \tag{1}$$

PTI score

Definition

We defined the PTI score (Figure 1A) according to Equations 2 and 3.

$$\sum_{i=1}^{n} l_{\mathrm{sPTI}i} = l_{\mathrm{sPTI1}} + l_{\mathrm{sPTI2}} + \cdots + l_{\mathrm{sPTI}k} + \cdots + l_{\mathrm{sPTI}n} \tag{2}$$

$$\text{PTI score} = \frac{l_{\mathrm{pPTI}}}{l_{\mathrm{pPTI}} + \sum_{i=1}^{n} l_{\mathrm{sPTI}i}} \tag{3}$$

where $l_{\mathrm{pPTI}} + \sum_{i=1}^{n} l_{\mathrm{sPTI}i}$ represents the sum of all PTI lengths.

The definition is derived from the hypothesis that the potential for translation of a pPTI is reduced by translation of sPTIs. Consistent with this hypothesis, coding transcripts with translation of sPTIs had lower PTI scores than all coding transcripts (Figure 2C).

Example

586 For an RNA sequence with only one PTI, the PTI score is 1 (Figure 1B). An RNA
587 sequence with many sPTIs tended to have a score close to 0 (Figure 1B). If the sum of
588 all sPTI lengths was equal to pPTI length, the PTI score is 0.5 (Figure 1B). The PTI
589 score of the *NCYM* transcript is 0.568 (Supplementary Figure 1C). Further information
590 is included in the Supplementary Notes.

591 ***Characteristics***

592 Therefore, the range of the PTI score is:

593 $$0 < \text{PTI score} \leq 1 \quad (4)$$

594

595 **Relative frequencies *f*(*x*) and *g*(*x*)**

596 ***Definition***

597 We defined the, *f*(*x*) and *g*(*x*), respectively, as (Figure 1C):

598 $$f(x) = \frac{NM(x)}{TNM} \quad (5)$$

599 $$g(x) = \frac{NR(x)}{TNR} \quad (6)$$

600 where TNM and TNR represent the total numbers of coding and noncoding
601 transcripts, respectively, excluding transcripts lacking PTIs. *NM*(*x*) and *NR*(*x*) are the
602 numbers of coding and noncoding transcripts with a PTI score of *x*, respectively.
603 To define coding/non-coding transcripts with a PTI score of *x*, we divided the
604 histograms into ten classes, and used the median values of the classes to represent the
605 PTI score (Figure 1C). Therefore, in Equations 5 and 6, the PTI score *x* is restricted as
606 follows:

$$x = 0.05, 0.15, 0.25, 0.35, 0.45, 0.55, 0.65, 0.75, 0.85, \text{or } 0.95 \quad (7)$$

Characteristics

Thus, $f(x)$ and $g(x)$ follow Equations 8–11:

$$0 \leq f(x) \leq 1 \quad (8)$$

$$0 \leq g(x) \leq 1 \quad (9)$$

$$\sum_x f(x) = 1 \quad (10)$$

$$\sum_x g(x) = 1 \quad (11)$$

Overlapping scores O_{pti} and O_{cov}

Definition

The $O(x)$ was calculated according to Equation 12:

$$O(x) = \sum_x o(x) \quad (12)$$

where $o(x)$ is the smaller value of the relative frequency of coding $f(x)$ or noncoding transcripts $g(x)$. O_{pti} is $O(x)$ with PTI score = x, and O_{cov} is $O(x)$ with ORF coverage = x.

Protein-coding potential $F(x)$

Definition

$F(x)$ was calculated according to Equation 13:

629 $$F(x) = \frac{f(\mathrm{x})}{f(\mathrm{x})+g(\mathrm{x})} \quad (13)$$

630 ***Example***

631 For example, $F(0.15)$ in human transcripts is shown in Figure 1D. $F(0.15)$ was

632 calculated using Equation 13, as follows:

633 $$f(0.15) = 0.060$$

634 $$g(0.15) = 0.268$$

635 $$F(0.15) = \frac{f(0.15)}{f(0.15)+g(0.15)} = \frac{0.060}{0.060+0.268} = 0.18292 = 0.183$$

636

637 **Identification of noncoding transcripts with high protein-coding potential**

638 NR transcripts with high $F(x)$ ($0.6 \leq x < 0.8$) were identified from the total NR

639 transcripts from the NCBI nucleotide database. NR transcripts shorter than 200

640 nucleotides or with pPTIs encoding putative peptides with fewer than 20 residues were

641 excluded. The amino acid sequences of pPTIs in these transcripts were subjected to a

642 BLASTP search to detect the presence of putative domain structures. In the BLASTP

643 search, non-redundant protein sequences (nr) were applied as the search set, and quick

644 accelerated protein-protein BLAST (BLASTP) was chosen as the algorithm. In the

645 search results, putative conserved domains or the message "No putative conserved

646 domains have been detected" are shown in the Graphical Summary tab.

647 CDSEARCH/cdd was used to search for conserved domain structures using the default

648 settings: low-complexity filter, no; composition-based adjustment, yes; E-value

649 threshold, 0.01; maximum number of hits, 500. Based on these data, transcripts with or
650 without putative conserved domain structures are indicated as + or -, respectively.
651
652 **Functional annotation of original genes**
653 Original genes were defined as those noted in the official gene name of NR transcripts,
654 including sense genes for antisense transcripts, homologous genes for pseudogenes,
655 coding genes for noncoding transcript variants, and readthrough, divergent, or intronic
656 transcripts. For lincRNAs, miRNA host genes, small nuclear RNAs, and other
657 lncRNAs, the official gene symbol was used for annotation. This information was
658 manually checked using the information available in the nucleotide database. The
659 DAVID program (https://www.david.ncifcrf.gov) was used to identify the enriched
660 molecular functions and pathways related to the original genes. *Q*-values (*P*-values
661 adjusted for false discovery rate) were calculated using the Benjamini–Hochberg
662 method in DAVID.
663
664 **Nonsynonymous (*K*a) to synonymous (*K*s) nucleotide substitution ratios**
665 To identify orthologous regions between human transcripts and chimpanzee/mouse
666 genomes, BLAT v. 36 (Kent 2002) was conducted using human transcript sequences
667 with the estimated PTI score against chimpanzee (PtRV2) and mouse (GRCm38.p6)
668 genomic sequences defined in the NCBI database. We defined the blat best-hit genomic
669 regions of chimpanzee/mouse as orthologs for each human transcript. The human–
670 chimpanzee (or human–mouse) sequences were aligned for each exon region and the

671 sequences were combined for each transcript. Only orthologous sequence pairs of more
672 than 60 bp in length (encoding > 20 amino acid residues) were extracted.
673 Nonsynonymous (*K*a) and synonymous (*K*s) nucleotide substitution rates were
674 estimated as described by Yang and Nielsen (Yang and Nielsen 2000), implemented in
675 PAML version 4.8a (Yang 1997). Transcripts with high *K*a (> 1) or high *K*s (> 1) were
676 excluded from our dataset as outliers. We calculated *K*a and *K*s for 47,228 NM human–
677 chimpanzee, 14,116 NM human–mouse, 8,810 NR human–chimpanzee, and 1,561 NR
678 human–mouse pairs.
679

680 **Relative frequencies of negatively selected genes**

681 We defined this frequency, $h(x)$, in coding and noncoding transcripts (Figure 1G), as
682 shown in Equation 14:

683 $$h(x) = \frac{Nns(x)}{TNor(x)} \quad (14)$$

684 where $TNor(x)$ represents the total number of coding or noncoding transcripts with
685 orthologous sequences at PTI score = x. $Nns(x)$ is the number of coding or noncoding
686 transcripts with *K*a/*K*s < 0.5 at PTI score = x. The PTI score x is restricted as shown in
687 Equation 7.
688

689 **Phylogenic trees**

690 TimeTree (Hedges et al. 2006) was used to draw trees using official species names.
691

692 **Selection of viruses and identification of vORFs**

693 The complete genomes of positive-sense single-stranded RNA viruses infecting humans
694 or bacteria (Supplementary Tables 14 and 15) were collected from the NCBI Virus
695 database (Hatcher et al. 2017). Viral ORFs were identified, and the sums of vORF
696 lengths $\sum_{i=1}^{n} l_{\mathrm{vORF}i}$ were manually calculated. We eliminated those viruses that
697 translated viral proteins after splicing or using exceptional translation mechanisms such
698 as ribosome frameshifting, alternative initiation sites, ribosome slippage, and RNA
699 editing.

700

701 **vORF score**

702 ***Definition***

703 The vORF score was calculated according to Equations 15–17:

704 $$\sum_{i=1}^{n} l_{\mathrm{vORF}i} = l_{\mathrm{vORF1}} + l_{\mathrm{vORF2}} + \cdots + l_{\mathrm{vORF}k} + \cdots + l_{\mathrm{vORF}n} \quad (15)$$

705 $$\sum_{i=1}^{n} l_{\mathrm{sPTI}i} = l_{\mathrm{sPTI1}} + l_{\mathrm{sPTI2}} + \ldots + l_{\mathrm{sPTI}k} + \ldots + l_{\mathrm{sPTI}n} \quad (16).$$

706 $$\text{vORF score} = \frac{\sum_{i=1}^{n} l_{\mathrm{vORF}i}}{\sum_{i=1}^{n} l_{\mathrm{vORF}i} + \sum_{i=1}^{n} l_{\mathrm{sPTI}i}} \quad (17)$$

707

708 where $l_{\mathrm{vORF}i}$ represents the length of the bona fide ORFs, and $\sum_{i=1}^{n} l_{\mathrm{sPTI}i}$ is the sum of
709 the lengths of the secondary PTI lengths. $\sum_{i=1}^{n} l_{\mathrm{vORF}i} + \sum_{i=1}^{n} l_{\mathrm{sPTI}i}$ represents the sum
710 of the lengths of all PTIs, including all ORFs.

711

712 **PTI score calculations using transcriptome data**

713 Transcriptome data from five species were obtained from a previous study (Sarropoulos
714 et al. 2019). All transcripts expressed at detectable levels (non-zero) in each tissue were
715 used to calculate PTI scores for lncRNAs and to plot PTI score distributions. For the
716 correlation between tissue specificity and PTI score, we divided the transcripts into the
717 indicated groups according to the number of tissues in which the transcript was detected
718 and described the PTI score distribution in each group. Human transcriptome data for
719 coding transcripts were obtained from the Human Protein Atlas
720 (http://www.proteinatlas.org), including RNA isoform data from 131 cell lines and 281
721 tissues. The PTI score for each transcript was calculated from Ensembl data.
722

723 **Statistical analyses**

724 Statistical analyses were performed using Excel and R software (R Project for Statistical
725 Computing, Vienna, Austria).
726

727 **Data availability**

728 1. Source data for statistical analyses and figures (10 example datasets):
729 https://figshare.com/s/498cb340a075284b2dbf
730 2. Code associated with generating and analyzing these tables:
731 https://figshare.com/s/0f1ed0954d5bd620eb59
732

733 **Acknowledgments**

We thank Yohko Yamaguchi, Yoshitaka Hippo, Sana Yokoi, and Akira Nakagawara for their helpful comments; Isao Kurosaka and Miayamoto Joe Philips for assistance in calculating PTI scores, and Mayuko Seto, Ryo Ohtaka, Manami Shinbori, Abedin Swapnil Eishraq, Kanna Kamikawa, and Taichi Yokoi for assistance in checking putative domain structures using BLASTP and classification of species according to the IUCN Red List. This work was partially supported by the Yasuda Medical Foundation, Takeda Science Foundation, and Interstellar Initiative grant18jm0610006h0001 to Y.S. from the Japan Agency for Medical Research and Development.

Author contributions

Y.S. conceived and developed the research plan; Y.S., M.K., M.N., K.N., H.K., M.K., and T.M. analyzed the data; and Y.S., M.K., and T.M. wrote the manuscript.

Additional information

Supplementary information is available.

Competing interests

The authors declare no competing financial interests.

754 **References**

755

756 Ankarklev J, Jerlström-Hultqvist J, Ringqvist E, Troell K, Svärd SG. 2010. Behind
757 the smile: cell biology and disease mechanisms of Giardia species. *Nat Rev*
758 *Microbiol*. 8:413–422.

759

760 Bartelt LA, Sartor RB. 2015. Advances in understanding Giardia: determinants and
761 mechanisms of chronic sequelae. *F1000Prime Rep*. 7:62.

762

763 Bazzini AA, Johnstone TG, Christiano R, Mackowiak SD, Obermayer B, Fleming
764 ES, Vejnar CE, Lee MT, Rajewsky N, Walther TC, et al. 2014. Identification of
765 small ORFs in vertebrates using ribosome footprinting and evolutionary
766 conservation. *EMBO J*. 33:981–993.

767

768 Begun DJ, Lindfors HA, Thompson ME, Holloway AK. 2006. Recently evolved
769 genes identified from Drosophila yakuba and D. erecta accessory gland expressed
770 sequence tags. *Genetics*. 172:1675–1681.

771

772 Begun DJ, Lindfors HA, Kern AD, Jones CD. 2007. Evidence for de novo evolution
773 of testis-expressed genes in the drosophila yakuba/drosophila erecta clade. *Genetics*.
774 176:1131–1137.

775

776 Brown SA, Warburton D, Brown LY, Yu CY, Roeder ER, Stengel-Rutkowski S,
777 Hennekam RC, Muenke M. 1998. Holoprosencephaly due to mutations in ZIC2, a
778 homologue of Drosophila odd-paired. *Nat Genet.* 20:180–183.

779

780 Buret AG, Cacciò SM, Favennec L, Svärd S. 2020. Update on Giardia: Highlights
781 from the seventh International Giardia and Cryptosporidium Conference. Mise à
782 jour sur Giardia et la giardiase: faits saillants de la Septième Conférence
783 Internationale sur Giardia et Cryptosporidium. *Parasite.* 27:49.

784

785 Candeias MM. 2011. The can and can't dos of p53 RNA. *Biochimie.* 93:1962–1965.

786

Chen S, Krinsky BH, Long M. 2013. New genes as drivers of phenotypic evolution. New genes as drivers of phenotypic evolution. *Nat Rev Genet*. 14:645–660.

Calvo SE, Pagliarini DJ, Mootha VK. 2009. Upstream open reading frames cause widespread reduction of protein expression and are polymorphic among humans. *Proc Natl Acad Sci U S A*. 106(18):7507-12. doi: 10.1073/pnas.0810916106. Epub 2009 Apr 16. PMID: 19372376; PMCID: PMC2669787.

Djebali S, Davis CA, Merkel A, Dobin A, Lassermann T, Mortazavi A, Tanzer A, Lagarde J, Lin W, Schlesinger F, Xue C, et al. 2012. Landscape of transcription in human cells. *Nature.* 489:101–108.

Douka K, Birds I, Wang D, Kosteletos A, Clayton S, Byford A, Vasconcelos EJR, O'Connell MJ, Deuchars J, Whitehouse A, Aspden JL. 2021. Cytoplasmic long noncoding RNAs are differentially regulated and translated during human neuronal differentiation. *RNA*. 27:1082-1101. doi: 10.1261/rna.078782.121. Epub 2021 Jun 30. PMID: 34193551; PMCID: PMC8370745.

Frankham R, Bradshaw CJA, Brook BW. 2014. Genetics in conservation management: Revised recommendations for the 50/500 rules, Red List criteria and population viability analyses. *Biological Conservation*. 170: 56-63. https://doi.org/10.1016/j.biocon.2013.12.036.

French SL, Santangelo TJ, Beyer AL, Reeve JN. 2007. Transcription and translation are coupled in Archaea. *Mol Biol Evol*. 24:893–895.

Frith MC, Forrest AR, Nourbakhsh E, Pang KC, Kawai J, Carninci P, Hayashizaki Y, Ingolia NT, Lareau LF, Weissman JS. 2011. Ribosome profiling of mouse embryonic stem cells reveals the complexity and dynamics of mammalian proteomes. *Cell.* 147:789–802.

Gripp KW, Wotton D, Edwards MC, Roessler E, Ades L, Meinecke P, Richieri-Costa A, Zackai EH, Massagué J, Muenke M, et al. 2000. Mutations in TGIF cause

holoprosencephaly and link NODAL signalling to human neural axis determination. *Nat Genet*. 25:205–208.

Hatcher EL, Zhdanov SA, Bao Y, Blinkova O, Nawrocki EP, Ostapchuck Y, Schäffer AA, Brister JR. 2017. Virus Variation Resource - improved response to emergent viral outbreaks. *Nucleic Acids Res*. 45:D482-D490.

Hedges SB, Dudley J, Kumar S. 2006. TimeTree: A public knowledge-base of divergence times among organisms. *Bioinformatics.* 22: 2971-2972.

Holland PW, Marlétaz F, Maeso I, Dunwell TL, Paps J. 2017. New genes from old: asymmetric divergence of gene duplicates and the evolution of development. *Philos Trans R Soc Lond B Biol Sci*. 372:20150480.

Huang DW, Sherman BT, Lempicki RA. 2009a. Systematic and integrative analysis of large gene lists using DAVID bioinformatics resources. *Nat Protoc.* 4:44–57.

Huang DW, Sherman BT, Lempicki RA. 2009b. Bioinformatics enrichment tools: paths toward the comprehensive functional analysis of large gene lists. *Nucleic Acids Res.* 37:1–13.

Huang JZ, Chen M, Chen D, Gao X-C, Zhu S, Huang H, Hu M, Zhu H, Yan G-R. 2017. A peptide encoded by a putative lncRNA HOXB-AS3 suppresses colon cancer growth. *Mol Cell.* 68: 171–184.

Huang Y, Wang J, Zhao Y, Wang H, Liu T, Li Y, Cui T, Li W, Feng Y, Luo J, Gong J, Ning L, Zhang Y, Wang D, Zhang Y. 2021. cncRNAdb: a manually curated resource of experimentally supported RNAs with both protein-coding and noncoding function. *Nucleic Acids Res.* 49(D1):D65-D70. doi: 10.1093/nar/gkaa791. PMID: 33010163; PMCID: PMC7778915.

Ingolia NT, Lareau LF, Weissman JS. 2011. Ribosome profiling of mouse

embryonic stem cells reveals the complexity and dynamics of mammalian proteomes. *Cell*. 147: 789-802.

Ingolia NT. 2014. Ribosome profiling: new views of translation, from single codons to genome scale. *Nat Rev Genet*. 15:205–213.

Islam SM, Suenaga Y, Takatori A, Ueda Y, Kaneko Y, Kawana H, Itami M, Ohira M, Yokoi S, Nakagawara A. 2015. Sendai virus-mediated expression of reprogramming factors promotes plasticity of human neuroblastoma cells. *Cancer Sci.* 106:1351–1361.

Kaessmann H. 2010. Origins, evolution, and phenotypic impact of new genes. *Genome Res*. 20:1313-26. doi: 10.1101/gr.101386.109. Epub 2010 Jul 22. PMID: 20651121; PMCID: PMC2945180.

Kaiser VB, Talmane L, Kumar Y, Semple F, MacLennan M; Deciphering Developmental Disorders Study, FitzPatrick DR, Taylor MS, Semple CA. 2021. Mutational bias in spermatogonia impacts the anatomy of regulatory sites in the human genome. *Genome Res*. Aug 20. doi: 10.1101/gr.275407.121. Epub ahead of print. PMID: 34417209.

Kaneko Y, Suenaga Y, Islam SM, Matsumoto D, Nakamura Y, Ohira M, Yokoi S, Nakagawara A. 2015. Functional interplay between MYCN, NCYM and OCT4 promotes aggressiveness of human neuroblastomas. *Cancer Sci.* 106:840–847.

Kanatsu-Shinohara M, Tanaka T, Ogonuki N, Ogura A, Morimoto H, Cheng PF, Eisenman RN, Trumpp A, Shinohara T. 2016. Myc/Mycn-mediated glycolysis enhances mouse spermatogonial stem cell self-renewal. *Genes Dev*. 30:2637-2648. doi: 10.1101/gad.287045.116. PMID: 28007786; PMCID: PMC5204355.

Kato K, Miya F, Hamada N, Negishi Y, Narumi-Kishimoto Y, Ozawa H, Ito H, Hori I, Hattori A, Okamoto N, et al. 2019. *MYCN* de novo gain-of-function mutation in a patient with a novel megalencephaly syndrome. *J Med Genet.* 56:388-395.

Kent WJ. 2002. BLAT--the BLAST-like alignment tool. *Genome Res*. 12:656–664.

Kimura M. 1968. Evolutionary rate at the molecular level. *Nature*. 217:624-6. doi: 10.1038/217624a0. PMID: 5637732.

Kimura, M. (1983). *The Neutral Theory of Molecular Evolution*. Cambridge: Cambridge University Press. doi:10.1017/CBO9780511623486

Kloc M, Foreman V, Reddy SA. 2011. Binary function of mRNA. *Biochimie.* 93:1955–1961.

Knowles DG, McLysaght A. 2009. Recent de novo origin of human protein-coding genes. *Genome Res*. 19:1752–1759.

Kopp F, Mendell JT. 2018. Functional classification and experimental dissection of long noncoding RNAs. *Cell*. 172:393–407.

Levine MT, Jones CD, Kern AD, Lindfors HA, Begun DJ. 2006. Novel genes derived from noncoding DNA in drosophila melanogaster are frequently X-linked and exhibit testis-biased expression. *Proc Natl Acad Sci U S A*. 103:9935–9939.

Li L, Foster CM, Gan Q, Nettleton D, James MG, Myers AM, Wurtele ES. 2009. Identification of the novel protein QQS as a component of the starch metabolic network in Arabidopsis leaves. *Plant J*. 58:485–498.

Li D, Dong Y, Jiang Y, Jiang H, Cai J, Wang W. 2010. A de novo originated gene depresses budding yeast mating pathway and is repressed by the protein encoded by its antisense strand. *Cell Res*. 20:408–420.

Li C-Y, Zhang Y, Wang Z, Zhang Y, Cao C, Zhang PW, Lu SJ, Li X, Yu Q, Zheng X, et al. 2010. A human-specific de novo protein-coding gene associated with human brain functions. *PLoS Comput Biol*. 6:e1000734.

Li J, Liu C. 2019. Coding or noncoding, the converging concepts of RNAs. *Front Genet*. 10:496.

Lynch M. 2010 Evolution of the mutation rate. *Trends Genet*. 26:345-52. doi: 10.1016/j.tig.2010.05.003. Epub 2010 Jun 30. PMID: 20594608; PMCID: PMC2910838.

Lynch M, Ackerman MS, Gout JF, Long H, Sung W, Thomas WK, Foster PL. 2016. Genetic drift, selection and the evolution of the mutation rate. *Nat Rev Genet*. 17:704-714. doi: 10.1038/nrg.2016.104. PMID: 27739533.

McLysaght A, Guerzoni D. 2015. New genes from non-coding sequence: the role of *de novo* protein-coding genes in eukaryotic evolutionary innovation. *Philos Trans R Soc Lond B Biol Sci.* 370:20140332.

McLysaght A, Hurst LD. 2016. Open questions in the study of de novo genes: what, how and why. *Nat Rev Genet.* 17:567–578.

Miller OL Jr, Hamkalo BA, Thomas CA Jr. 1970. Visualization of bacterial genes in action. *Science.* 169:392–395.

Monsellier E, Chiti F. 2007. Prevention of amyloid-like aggregation as a driving force of protein evolution. *EMBO Rep*. 8:737–742.

Ohno S. 1970. Evolution by gene duplication. New York: Springer-Verlag.

Ohta T. 1992. The nearly neutral theory of molecular evolution. *Annu Rev Ecol Syst.* 23:263-86.

Okazaki Y, Furuno M, Kasukawa T, Adachi J, Bono H, Kondo S, Nikaido I, Osato N, Saito R, Suzuki H, et al.; FANTOM Consortium; RIKEN Genome Exploration

Research Group Phase I & II Team. 2002. Analysis of the mouse transcriptome based on functional annotation of 60,770 full-length cDNAs. *Nature*. 420:563–573.

Ruiz-Orera J, Messeguer X, Subirana JA, Alba MM. 2014. Long non-coding RNAs as a source of new peptides. *Elife.* 3:e03523.

Ruiz-Orera J, Verdaguer-Grau P, Villanueva-Cañas JL, Messeguer X, Albà MM. 2018. Translation of neutrally evolving peptides provides a basis for de novo gene evolution. *Nat Ecol Evol*. 2:890–896.

Sarropoulos I, Marin R, Cardoso-Moreira M, Kaessmann H. 2019. Developmental dynamics of lncRNAs across mammalian organs and species. *Nature*. 571:510-514. doi: 10.1038/s41586-019-1341-x. Epub 2019 Jun 26. PMID: 31243368; PMCID: PMC6660317.

Shoji W, Suenaga Y, Kaneko Y, Islam SM, Alagu J, Yokoi S, Nio M, Nakagawara A. 2015. NCYM promotes calpain-mediated Myc-nick production in human MYCN-amplified neuroblastoma cells. *Biochem Biophys Res Commun.* 461:501–506.

Suenaga Y, Islam SM, Alagu J, Kaneko Y, Kato M, Tanaka Y, Kawana H, Hossain S, Matsumoto D, Yamamoto M, et al. 2014. *NCYM*, a Cis-antisense gene of *MYCN*, encodes a de novo evolved protein that inhibits GSK3β resulting in the stabilization of MYCN in human neuroblastomas. *PLoS Genet.* 10:e1003996.

Suenaga Y, Nakatani K, Nakagawara A. 2020. De novo evolved gene product NCYM in the pathogenesis and clinical outcome of human neuroblastomas and other cancers. *Jpn J Clin Oncol*. 50: 839-846.

Sun L, Luo H, Bu D, Zhao G, Yu K, Zhang C, Liu Y, Chen R, Zhao Y. 2013. Utilizing sequence intrinsic composition to classify protein-coding and long non-coding transcripts. *Nucleic Acids Res*. 41:e166.

983 Toll-Riera M, Bosch N, Bellora N, Castelo R, Armengol L, Estivill X, Albà MM.
984 2009 Origin of primate orphan genes: a comparative genomics approach. *Mol Biol*
985 *Evol*. 26:603–612.
986
987 Ulitsky I, Bartel DP. 2013. lincRNAs: genomics, evolution, and mechanisms. *Cell*.
988 154:26–46.
989
990 van Bokhoven H, Celli J, van Reeuwijk J, Rinne T, Glaudemans B, van Beusekom
991 E, Rieu P, Newbury-Ecob RA, Chiang C, Brunner HG. 2005. MYCN
992 haploinsufficiency is associated with reduced brain size and intestinal atresias in
993 Feingold syndrome. *Nat Genet.* 37:465–467.
994
995 Van Oss SB, Carvunis AR. 2019. De novo gene birth. *PLoS Genet*. 15:e1008160.
996
997 Wang L, Park HJ, Dasari S, Wang S, Kocher JP, Li W. 2013. CPAT: Coding-
998 Potential Assessment Tool using an alignment-free logistic regression model.
999 *Nucleic Acids Res*. 41:e74.
1000
1001 Wilson BA, Foy SG, Neme R, Masel J. 2017. Young genes are highly disordered as
1002 predicted by the preadaptation hypothesis of de novo gene birth. *Nat Ecol Evol*.
1003 1:0146.
1004
1005 Wu Q, Wright M, Gogol MM, Bradford WD, Zhang N, Bazzini AA. 2020.
1006 Translation of small downstream ORFs enhances translation of canonical main open
1007 reading frames. *EMBO J*. 39:e104763. doi: 10.15252/embj.2020104763. Epub 2020
1008 Aug 3. PMID: 32744758; PMCID: PMC7459409.
1009
1010 Yang Z, Nielsen R. 2000. Estimating synonymous and nonsynonymous substitution
1011 rates under realistic evolutionary models. *Mol Biol Evol.* 17:32–43.
1012
1013 Yang Z. 1997. PAML: a program package for phylogenetic analysis by maximum
1014 likelihood. *Comput Appl Biosci*. 13:555–556
1015

Zhang YE, Long M. 2014. New genes contribute to genetic and phenotypic novelties in human evolution. *Curr Opin Genet Dev*. 29:90–96.

Zeng C, Hamada M. 2018. Identifying sequence features that drive ribosomal association for lncRNA. *BMC Genomics*. 19:906. doi: 10.1186/s12864-018-5275-8. PMID: 30598103; PMCID: PMC6311901.

1024

1025 **Table 1.** Numbers of original transcripts that produced NR transcripts with high coding

1026 frequency (0.6 ≤ PTI score < 0.8)

Transcript	Domain		Total	P-value
	With	Without		
Antisense	4	61	65	7.79E-08
LincRNA	3	65	68	7.60E-09
Pseudogene	50	17	67	4.32E-07
Readthrough	7	0	7	6.00E-03
Transcript variant of coding gene	146	35	181	1.05E-19
Divergent	0	2	2	N.S.
Intronic	0	6	6	N.S.
Small nuclear RNA	0	3	3	N.S.
miRNA host gene	0	3	3	N.S.
Other lncRNA	7	118	125	1.12E-13
Total	217	310	527	

1027 *P*-values were calculated using the Yate's continuity correction. N.S., not significant.

1028

1029 **Figure legends**

1030 **Figure 1. Potentially translated island (PTI) scores predict protein-coding potential**

1031 **of human transcripts.** (A) Conceptual schematic of PTIs in an RNA in the three

1032 reading frames and definition of PTI score. Black and white rectangles indicate primary

1033 and secondary PTIs, respectively. The primary PTI is the longest PTI, while secondary

1034 PTIs are all others; l is PTI length. (B) Schematic of PTI distributions in RNAs with

1035 low (0-0.5), medium (0.5), and high (1) scores. (C) Relative frequencies of PTI scores

1036 of coding f(x) and noncoding g(x) transcripts (upper) and of random controls (bottom).

1037 (D) Explanation of F(x) for a PTI score of 0.15. (E) PTI score correlations with protein-

1038 coding potential, $F(x)$, at PTI scores $\leq$ 0.65 (upper) and those in random controls

1039 (lower). (F) Relationship between PTI scores and percentages of NR transcripts re-

1040 registered as NM during the past 3 years. N.D., not detected. (G) Relationship between

1041 PTI scores and $F(x)$ in human transcripts syntenic to chimpanzee (upper left) or mouse

1042 (bottom left). The relative frequency of transcripts with negative selection $h(x)$ are

1043 plotted for each PTI score (upper and bottom right). The transcripts are syntenic to the

1044 genome of chimpanzee (upper right) or mouse (bottom right).The open circles indicate

1045 NR transcripts and the closed circles indicate NM transcripts.

1046

1047 **Figure 2. Translation effects on human PTI score distributions.** (A) PTI score

1048 distribution of lincRNAs translating small proteins (red line, n = 174) registered in the

1049 SmProt database (http://bioinfo.ibp.ac.cn/SmProt/) shifts to higher scores relative to all

1050 lincRNAs registered in Ensembl (black line, n = 11,875). (B) Locations of uORF (blue),

1051 sORF(red), and dORF(green) relative to major ORF (black). (C) PTI score distributions
1052 of coding transcripts with translation of uORF (blue, n =170), sORF (red, n = 1,698),
1053 and dORF (green, n = 98) compared to all coding transcripts registered in Ensembl
1054 (black, n = 94,039).
1055
1056 **Figure 3. Phylogenetic tree.** Numbers of species are indicated in each lineage. The
1057 lineages of five species, including one archaea (*Nitrososphaera viennensis* EN76), two
1058 fungi (*Puccinia graminis f. sp. Tritici* and *Pyricularia oryzae*), and two animals
1059 (*Strongylocentrotus purpuratus* and *Lingula anatine*) are unknown and excluded from
1060 the figure.
1061
1062 **Figure 4**. **Relationships between PTI scores and relative frequencies of coding and**
1063 **noncoding transcripts from bacteria to mammals**. Histograms of $f(x)$ (white) or $g(x)$
1064 (black) in observed data (left) and in nucleic-acid–scrambled controls (right) for each
1065 species analyzed. PTI scores with the highest $f(x)$ are presented in the histograms. O_{pti}
1066 was calculated using the PTI score distribution from observed data and indicated in the
1067 left panels.
1068
1069 **Figure 5. Relationships between PTI score and relative frequencies of coding f(x)**
1070 **and noncoding transcripts in Primates (A), Glires (B), and Laurasiatheria (C).**
1071

1072 **Figure 6. Overlap of PTI score distributions is negatively correlated with effective**
1073 **population sizes.** (A) Inversely proportional relationship between genome-wide
1074 mutation rates in protein-coding DNA per generation (U_p) and effective population sizes
1075 (N_e) in 24 species (left upper). Values are from Lynch et al., 2016. O_{pti} positively and
1076 negatively correlates with U_p (left bottom) and N_e (right upper); these relationships are
1077 approximated by logaritic and exponential functions, respectively. White, gray, and
1078 black dots indicate bacteria, unicellular eukaryotes, and multicellular eukaryotes,
1079 respectively. (B) O_{pti} is increased in vertebrates at risk of extinction (left) and with
1080 decreasing population trends (right). LC, least concern (n = 20); NT, near threatened (n
1081 = 3); VU, vulnerable (n = 1); EN, endangered (n = 5); CR, critically endangered (n = 5);
1082 EX, extinct (n = 1). *P*-values were calculated by the Mann–Whitney U test.
1083
1084 **Figure 7. Relationship between PTI score and protein-coding potential *F*(*x*) for 32**
1085 **eukaryotes.** Phylogenetic tree including the 32 species (left), dot plots, and shape and
1086 formulas of approximate functions. L and C indicate linear (in black) and constant (in
1087 red) functions. Fewer than five lncRNAs had a PTI score of 0.05 in *U. americanus*, *C.*
1088 *canadensis*, and *G. gorilla*; therefore, we eliminated the *F*(0.05) for these species for
1089 linear function approximations (asterisks). O_{pti} was calculated using PTI score
1090 distributions of observed data.
1091
1092 **Figure 8. Molecular mechanisms that affect PTI score distributions.** (A) Schematic
1093 explanation of sPTI length and bona fide viral ORFs in a (+) ssRNA virus genome and

1094 the definition of viral ORF (vORF) score. Black and white rectangles indicate viral

1095 ORFs and secondary PTIs, respectively. l is the length of the ORFs and PTIs. (B)

1096 Histograms of relative frequencies of human (+) ssRNA viruses (red) and

1097 bacteriophages (black). (C) PTI score distributions of lncRNAs in human tissues.

1098 Distributions in mature testes and other tissues are indicated as black and gray lines,

1099 respectively. (D) The relationship between tissue-specificity and PTI score distributions

1100 in humans. Line intensity represent specificity of gene expression.

1101

1102 **Figure 9. Hypothesis: new gene birth is a countermeasure to decline in effective**

1103 **population size.** (A) Schematic explaining how nuclear evolution and multicellularity

1104 contribute to the generation of noncoding RNAs with high PTI scores in eukaryotes. (B)

1105 Schematic illustrating new gene birth in response to decline in effective population size

1106 caused by environmental changes.

1107

1108

1109 **Supplementary figure legends**

1110 **Supplementary Figure 1. PTIs of *NCYM* and an example of PTI score calculation.**

1111 (A) *NCYM* cDNA sequence. (B) Coding prediction of *NCYM* by CPAT

1112 (http://lilab.research.bcm.edu). (C) Translated amino-acid sequence of *NCYM* in 3

1113 frames in the 5′ to 3′ (sense) direction. Red characters, primary PTI; blue characters,

1114 secondary PTIs. Stop codons are shown as asterisks. (D) Calculation of PTI score and

1115 $F(x)$ for the *NCYM* transcripts. The length of pPTI is 109 and the sum of sPTI lengths is

1116 83; therefore, the PTI score is 0.568.

1117

1118 **Supplementary Figure 2. Relationships between relative frequencies of coding and**

1119 **noncoding transcripts for human and mouse PTI scores.** (A) Histogram of PTI score

1120 relative frequencies in coding $f(x)$ and noncoding $g(x)$ human transcripts with random

1121 shuffling controls using human data sets from RefSeq. (B) Relative frequencies of

1122 coding $f(x)$ and noncoding $g(x)$ transcripts calculated using human data sets from

1123 Ensembl. (B) Relative frequencies of coding $f(x)$ and noncoding $g(x)$ transcripts

1124 calculated using mouse data sets from RefSeq (upper panels) or Ensembl (lower

1125 panels).

1126

1127 **Supplementary Figure 3. PTI scores correlate with protein-coding potential, $F(x)$,**

1128 **at PTI scores $\leq$ 0.65 for human and mouse transcripts.** (A) Relationship between

1129 PTI score and $F(x)$ in a human data set from Ensemble and random controls (center).

1130 Random shuffling controls (right) were generated from a human data set from both

1131 Ensemble and RefSeq. (B) Relationships between PTI score and $F(x)$ in mouse

1132 transcripts using data sets from RefSeq (upper panels) or Ensembl (lower panels).

1133

1134 **Supplementary Figure 4. Effects of translation on distributions of ORF coverage**

1135 **and size in human lincRNAs.** ORF coverage (A) and ORF size (B) distributions of

1136 lincRNAs encoding small proteins (red line, n = 174) registered in the SmProt database

1137 (http://bioinfo.ibp.ac.cn/SmProt/) compared with all lincRNAs registered in Ensembl

1138 (black line, n = 11,875).

1139

1140 **Supplementary Figure 5. Translation of sPTI affects on human PTI score**

1141 **distributions.** PTI score distributions of coding transcripts with translation of uORFs

1142 (blue, n = 14,506), sORFs (red, n = 80), and dORFs (green, n = 3,955) registered in the

1143 sORF database (http://www.sorfs.org/), compared to all coding transcripts registered in

1144 Ensembl (black, n = 94,039).

1145

1146 **Supplementary Figure 6. Relationships between PTI scores and relative**

1147 **frequencies of coding and noncoding transcripts in archaea**. Phylogenetic tree for 9

1148 archaeal species and histogram of $f(x)$ (white) or $g(x)$ (black) in the data (left) and in

1149 nucleic-acid–scrambled controls (right). PTI scores with highest $f(x)$ are indicated in the

1150 histograms. The lineage of one archaea species (*Nitrososphaera viennensis* EN76) is

1151 unknown and thus excluded from the phylogenic tree. O_{pti} was calculated using the PTI

1152 score distribution of observed data.

1153

1154 **Supplementary Figure 7. Relationships between PTI score and relative frequencies**

1155 **for coding and noncoding transcripts in plants.** Phylogenetic tree for 12 plants and

1156 histogram of $f(x)$ (white) or $g(x)$ (black) in the data (left) and in sequence–scrambled

1157 controls (right). PTI scores with highest $f(x)$ are indicated. O_{pti} was calculated using the

1158 PTI score distribution of observed data.

1159

1160 **Supplementary Figure 8. Relationships between PTI score and relative frequencies**

1161 **of coding and noncoding transcripts in species shown in Figure 6.** Phylogenetic tree

1162 for 24 cellular organisms and histograms of $f(x)$ (white) or $g(x)$ (black) for PTI scores

1163 (left) and ORF coverage (right). O_{pti} and O_{cov} were calculated using the distribution of

1164 observed data.

1165

1166 **Supplementary Figure 9. Relationship between overlaps of ORF coverage**

1167 **distributions and effective population sizes.** Dot plots of O_{cov} and U_p (left) and N_e

1168 (right). These relationships are approximated by the logaritic and exponential functions,

1169 respectively. White, gray, and black dots indicate bacteria, unicellular eukaryotes, and

1170 multicellular eukaryotes, respectively.

1171

1172 **Supplementary Figure 10. Relationships between PTI scores and protein-coding**

1173 **potential $F(x)$ for 32 eukaryotes.** Data sets from Ensembl (left, used in Figure 7) and

1174 random controls (right). Mouse and human data are identical to those shown in

1175 Supplementary Figure 3. Shapes of approximate functions are shown as L or C,
1176 indicating linear (in black) and constant (in red) functions, respectively. Numbers of
1177 lncRNAs with PTI score 0.05 were < 5 in *U. americanus*, *C. canadensis*, and *G. gorilla*.
1178 Therefore, we eliminated the $F(0.05)$ from these species for the approximation by linear
1179 functions (asterisks).
1180
1181 **Supplementary Figure 11. PTI score distributions of lncRNAs from tissues from**
1182 **four mammals.** PTI score distributions for mature testes and other tissues are indicated
1183 as black and gray lines, respectively.
1184
1185 **Supplementary Figure 12. Relationships between tissue specificity and PTI score**
1186 **distributions for noncoding transcripts from four mammals.** Line intensity
1187 represents specificity of gene expression.
1188
1189 **Supplementary Figure 13. Relationships between tissue-specificity and PTI score**
1190 **distributions for coding transcripts from human cell lines (A) or tissues (B).** Line
1191 intensity represents specificity of gene expression.
1192
1193

1194 **Supplementary Table 1. Studied organisms with official names, taxonomic IDs,**

1195 **lineage information, and numbers of coding/noncoding transcripts.**

1196

1197 **Supplementary Table 2. Human NR transcripts reassigned as NM during the past**

1198 **three years.**

1199

1200 **Supplementary Table 3. Human NR transcripts with high protein-coding potential**

1201 **(0.6 ≤ PTI score < 0.8).**

1202

1203 **Supplementary Table 4. Functional annotation of human NR transcripts with high**

1204 **protein-coding potential and without putative domain structure(s).**

1205

1206 **Supplementary Table 5. Functional annotation of human NR transcripts with high**

1207 **protein-coding potential and with putative protein domain structure(s).**

1208

1209 **Supplementary Table 6. Mouse NR transcripts with high protein-coding potential**

1210 **(0.6 ≤ PTI score < 0.8).**

1211

1212 **Supplementary Table 7. Functional annotation of mouse NR transcripts with high**

1213 **protein-coding potential and without putative protein domain structure(s).**

1214

1215 **Supplementary Table 8. Functional annotation of mouse NR transcripts with high**

1216 **protein-coding potential and with putative domain structure(s).**

1217

1218 **Supplementary Table 9. NR transcripts with high protein-coding potential (0.6 ≤**

1219 **PTI score < 0.8) from *C. elegans*.**

1220

1221 **Supplementary Table 10. Functional annotation of NR transcripts with high**

1222 **protein-coding potential and without putative domain structure(s) from *C. elegans*.**

1223

1224 **Supplementary Table 11. Functional annotation of NR transcripts with high**

1225 **protein-coding potential and with putative domain structure(s) from *C. elegans*.**

1226

1227 **Supplementary Table 12. Twenty-three human noncoding transcripts showing**

1228 **both negative selection (*K*a/*K*s < 0.5) and high PTI scores.**

1229

1230 **Supplementary Table 13. Organisms shown in Figure 6 with official names,**

1231 **taxonomy IDs, lineage information, and numbers of coding or noncoding**

1232 **transcripts, O_{pti}, and O_{cov}. The effective population sizes (*N*e) and mutation rates**

1233 **(*U*p) were estimated by Lynch et al. (2016).**

1234

1235 **Supplementary Table 14. Positive-sense, single-stranded human viruses with**

1236 **official names, taxonomy IDs, lineage information, genome lengths, and sequences.**

1237

1238 **Supplementary Table 15. Positive-sense, single-stranded bacteriophages with**

1239 **official names, taxonomy IDs, lineage information, source information, genome**

1240 **lengths, and sequences.**

Figure 1

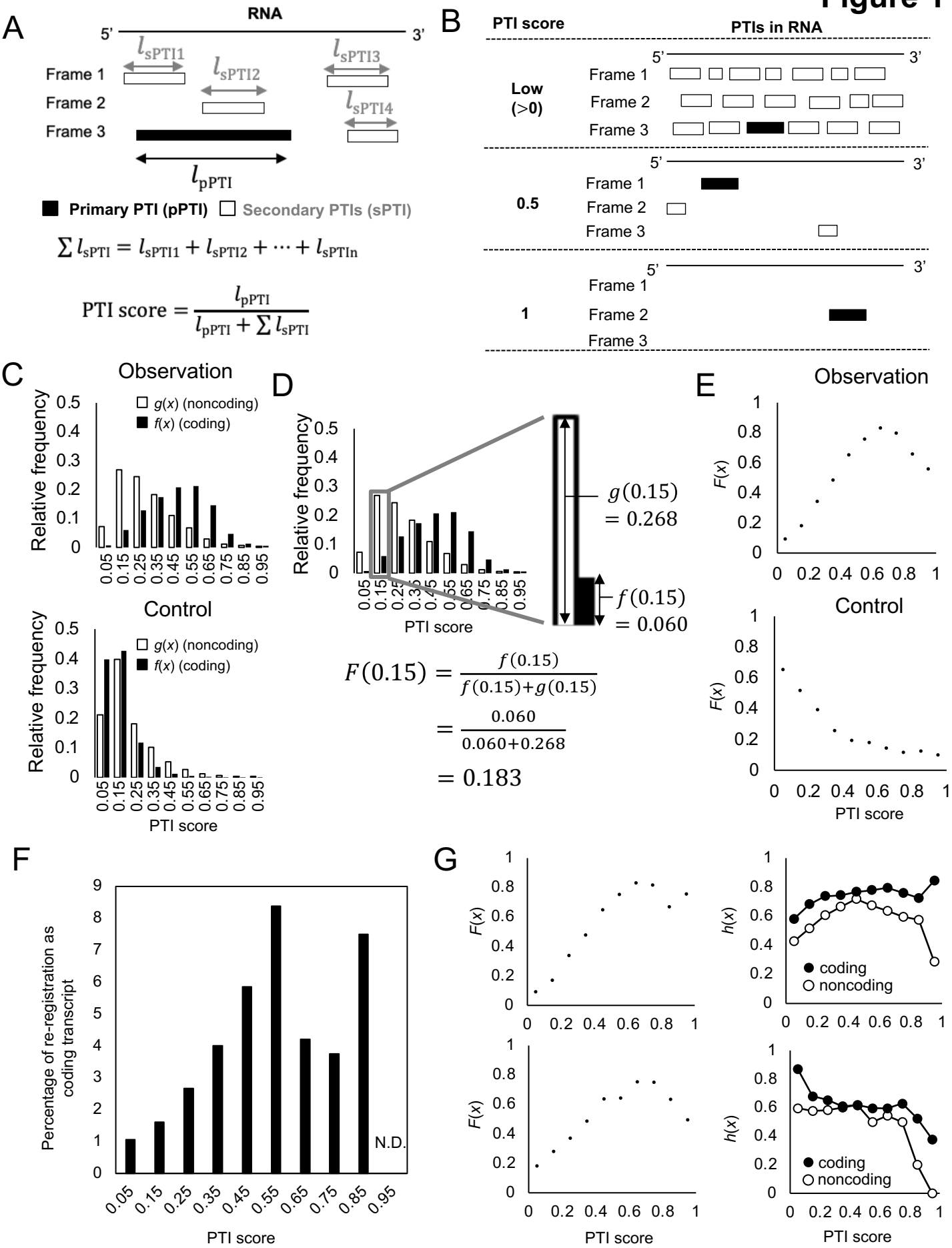

$$\sum l_{\mathrm{sPTI}} = l_{\mathrm{sPTI1}} + l_{\mathrm{sPTI2}} + \cdots + l_{\mathrm{sPTIn}}$$

$$\text{PTI score} = \frac{l_{\mathrm{pPTI}}}{l_{\mathrm{pPTI}} + \sum l_{\mathrm{sPTI}}}$$

$$F(0.15) = \frac{f(0.15)}{f(0.15)+g(0.15)} = \frac{0.060}{0.060+0.268} = 0.183$$

Figure 2

A

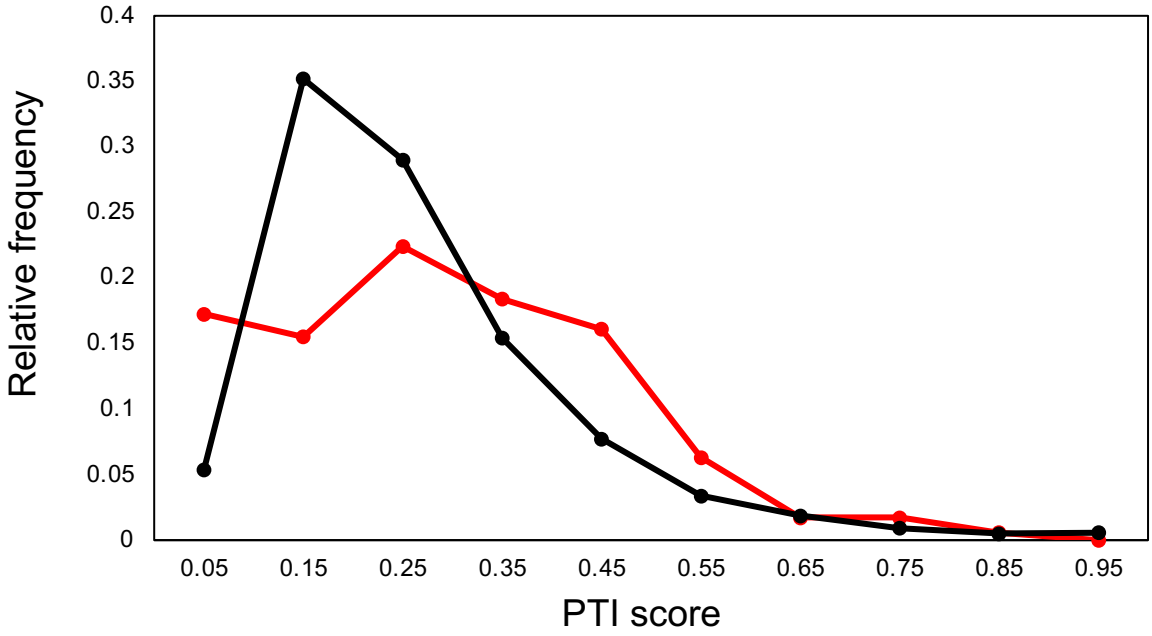
Relative frequency
0.4
0.35
0.3
0.25
0.2
0.15
0.1
0.05
0
0.05
0.15
0.25
0.35
0.45
0.55
0.65
0.75
0.85
0.95
PTI score

B

5'UTR
ORF
3'UTR
uORF
sORF
dORF

C

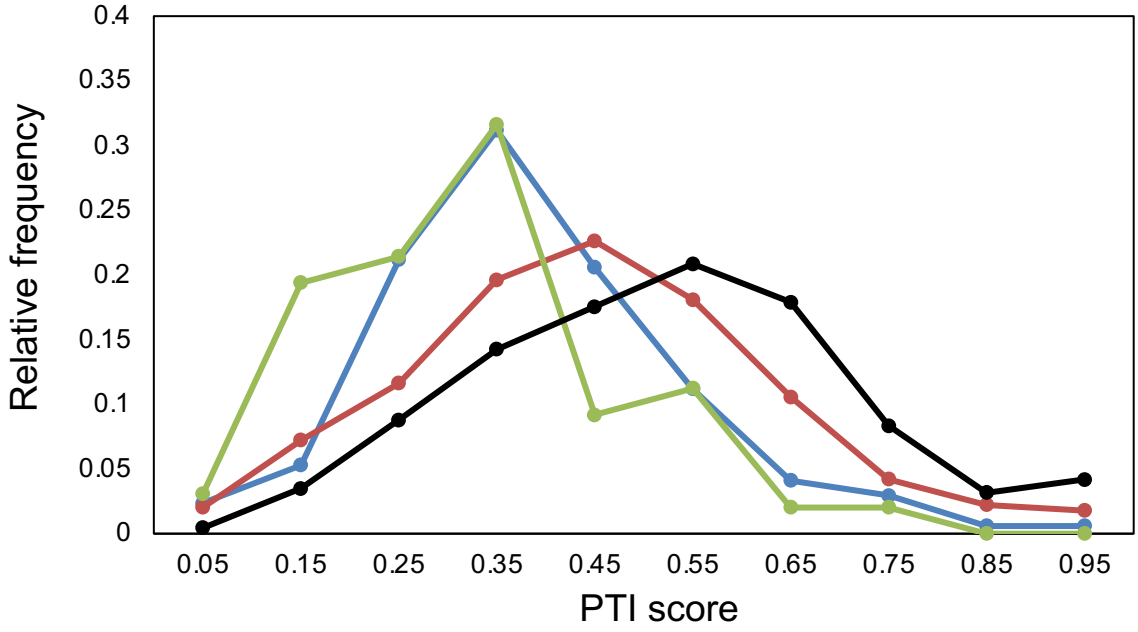
Relative frequency
0.4
0.35
0.3
0.25
0.2
0.15
0.1
0.05
0
0.05
0.15
0.25
0.35
0.45
0.55
0.65
0.75
0.85
0.95
PTI score

Figure 3

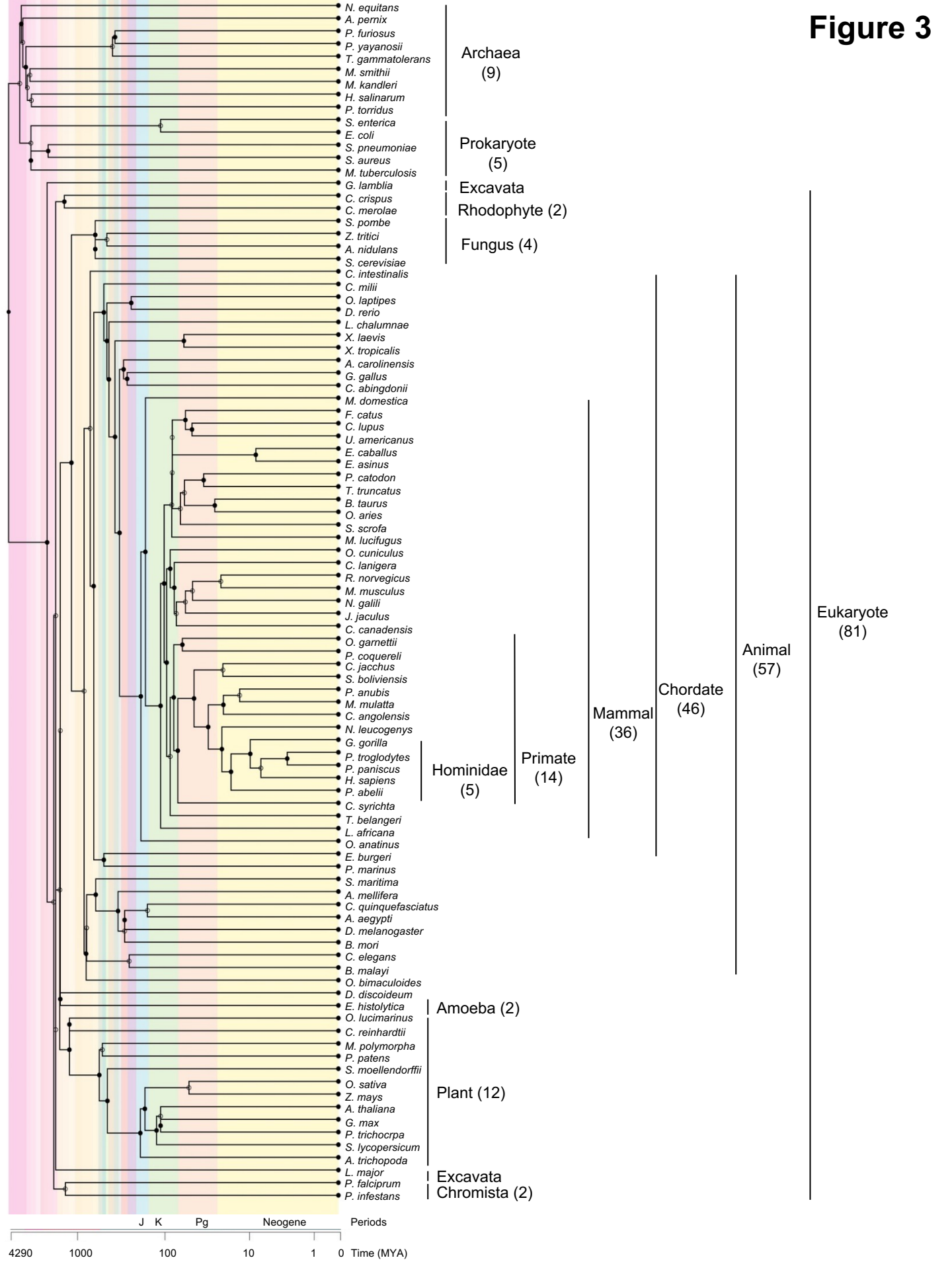
N. equitans
A. pernix
P. furiosus
P. yayanosii
T. gammatolerans
M. smithii
M. kandleri
H. salinarum
P. torridus
S. enterica
E. coli
S. pneumoniae
S. aureus
M. tuberculosis
G. lamblia
C. crispus
C. merolae
S. pombe
Z. tritici
A. nidulans
S. cerevisiae
C. intestinalis
C. milii
O. laptipes
D. rerio
L. chalumnae
X. laevis
X. tropicalis
A. carolinensis
G. gallus
C. abingdonii
M. domestica
F. catus
C. lupus
U. americanus
E. caballus
E. asinus
P. catodon
T. truncatus
B. taurus
O. aries
S. scrofa
M. lucifugus
O. cuniculus
C. lanigera
R. norvegicus
M. musculus
N. galili
J. jaculus
C. canadensis
O. garnettii
P. coquereli
C. jacchus
S. boliviensis
P. anubis
M. mulatta
C. angolensis
N. leucogenys
G. gorilla
P. troglodytes
P. paniscus
H. sapiens
P. abelii
C. syrichta
T. belangeri
L. africana
O. anatinus
E. burgeri
P. marinus
S. maritima
A. mellifera
C. quinquefasciatus
A. aegypti
D. melanogaster
B. mori
C. elegans
B. malayi
O. bimaculoides
D. discoideum
E. histolytica
O. lucimarinus
C. reinhardtii
M. polymorpha
P. patens
S. moellendorffii
O. sativa
Z. mays
A. thaliana
G. max
P. trichocrpa
S. lycopersicum
A. trichopoda
L. major
P. falciprum
P. infestans
Archaea (9)
Prokaryote (5)
Excavata
Rhodophyte (2)
Fungus (4)
Hominidae (5)
Primate (14)
Mammal (36)
Chordate (46)
Animal (57)
Eukaryote (81)
Amoeba (2)
Plant (12)
Excavata
Chromista (2)
J
K
Pg
Neogene
Periods
4290
1000
100
10
1
0
Time (MYA)

Figure 4

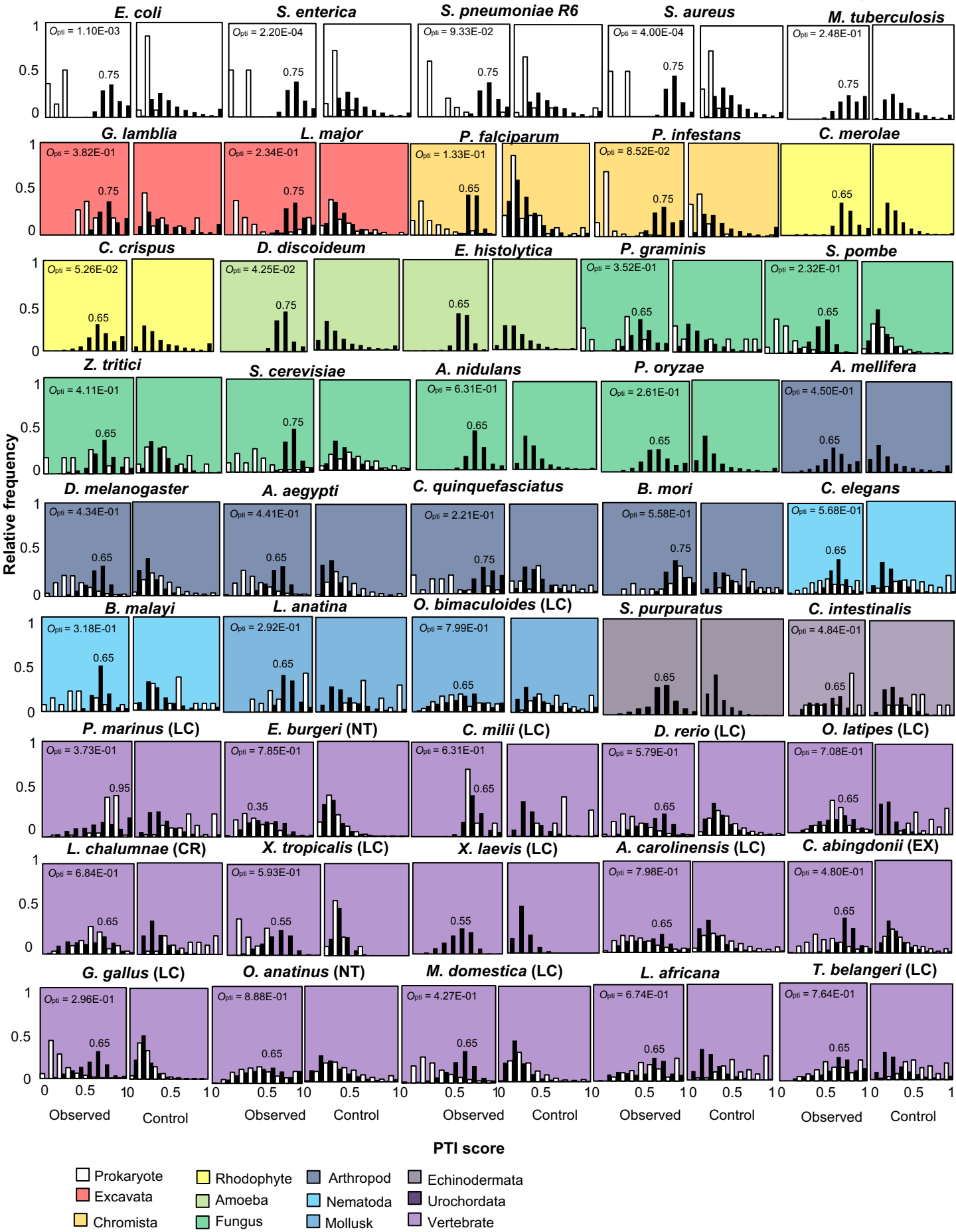
E. coli
Opti = 1.10E-03
0.75
S. enterica
Opti = 2.20E-04
0.75
S. pneumoniae R6
Opti = 9.33E-02
0.75
S. aureus
Opti = 4.00E-04
0.75
M. tuberculosis
Opti = 2.48E-01
0.75
G. lamblia
Opti = 3.82E-01
0.75
L. major
Opti = 2.34E-01
0.75
P. falciparum
Opti = 1.33E-01
0.65
P. infestans
Opti = 8.52E-02
0.75
C. merolae
0.65
C. crispus
Opti = 5.26E-02
0.65
D. discoideum
Opti = 4.25E-02
0.75
E. histolytica
0.65
P. graminis
Opti = 3.52E-01
0.65
S. pombe
Opti = 2.32E-01
0.65
Z. tritici
Opti = 4.11E-01
0.65
S. cerevisiae
0.75
A. nidulans
Opti = 6.31E-01
0.65
P. oryzae
Opti = 2.61E-01
0.65
A. mellifera
Opti = 4.50E-01
0.65
D. melanogaster
Opti = 4.34E-01
0.65
A. aegypti
Opti = 4.41E-01
0.65
C. quinquefasciatus
Opti = 2.21E-01
0.75
B. mori
Opti = 5.58E-01
0.75
C. elegans
Opti = 5.68E-01
0.65
B. malayi
Opti = 3.18E-01
0.65
L. anatina
Opti = 2.92E-01
0.65
O. bimaculoides (LC)
Opti = 7.99E-01
0.65
S. purpuratus
0.65
C. intestinalis
Opti = 4.84E-01
0.65
P. marinus (LC)
Opti = 3.73E-01
0.95
E. burgeri (NT)
Opti = 7.85E-01
0.35
C. milii (LC)
Opti = 6.31E-01
0.65
D. rerio (LC)
Opti = 5.79E-01
0.65
O. latipes (LC)
Opti = 7.08E-01
0.65
L. chalumnae (CR)
Opti = 6.84E-01
0.65
X. tropicalis (LC)
Opti = 5.93E-01
0.55
X. laevis (LC)
0.55
A. carolinensis (LC)
Opti = 7.98E-01
0.65
C. abingdonii (EX)
Opti = 4.80E-01
0.65
G. gallus (LC)
Opti = 2.96E-01
0.65
O. anatinus (NT)
Opti = 8.88E-01
0.65
M. domestica (LC)
Opti = 4.27E-01
0.65
L. africana
Opti = 6.74E-01
0.65
T. belangeri (LC)
Opti = 7.64E-01
0.65
Relative frequency
1
0.5
0
Observed
Control
PTI score
Prokaryote
Excavata
Chromista
Rhodophyte
Amoeba
Fungus
Arthropod
Nematoda
Mollusk
Echinodermata
Urochordata
Vertebrate

Figure 5

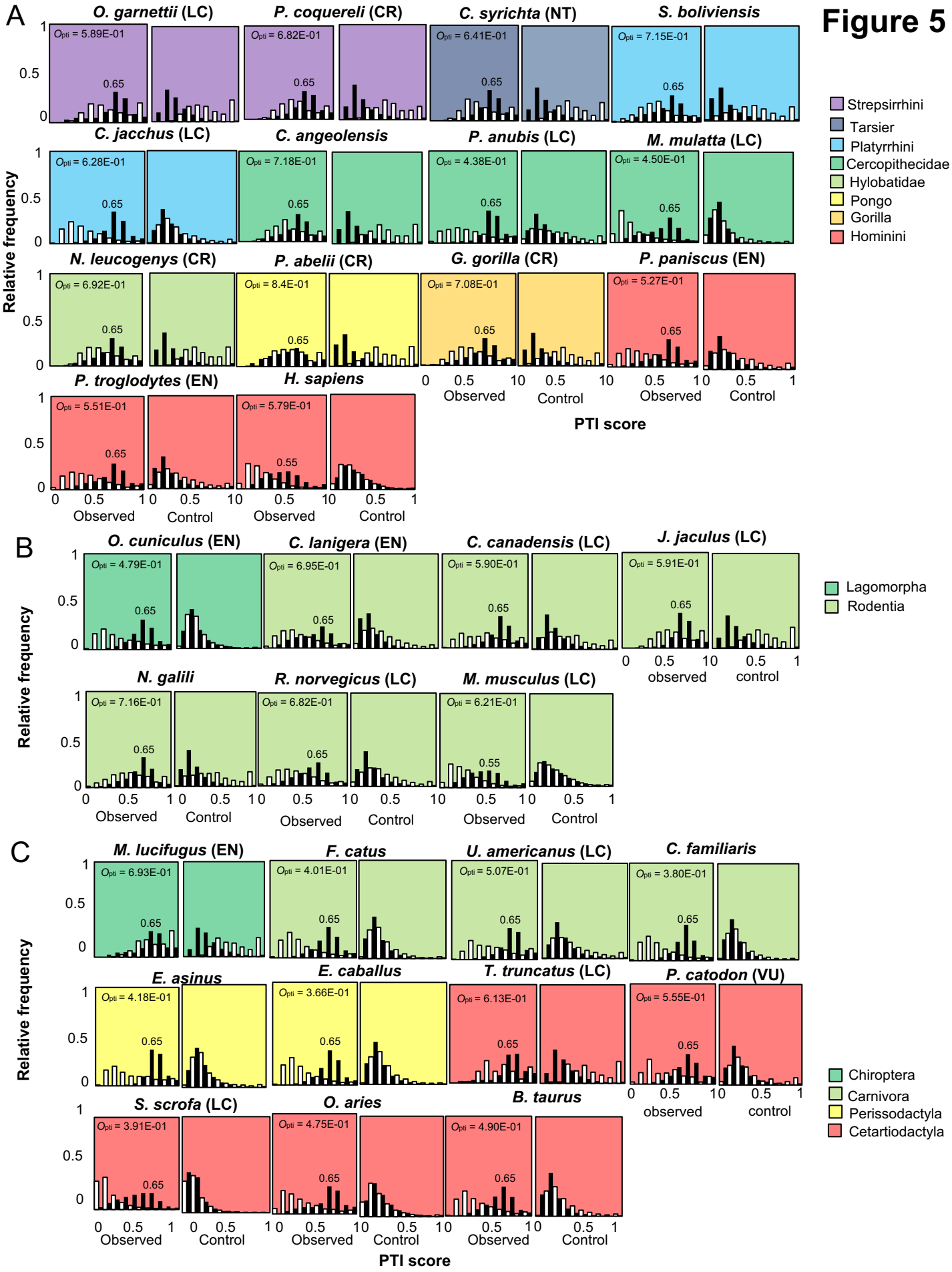
A
O. garnettii (LC)
Opti = 5.89E-01
P. coquereli (CR)
Opti = 6.82E-01
C. syrichta (NT)
Opti = 6.41E-01
S. boliviensis
Opti = 7.15E-01
C. jacchus (LC)
Opti = 6.28E-01
C. angeolensis
Opti = 7.18E-01
P. anubis (LC)
Opti = 4.38E-01
M. mulatta (LC)
Opti = 4.50E-01
N. leucogenys (CR)
Opti = 6.92E-01
P. abelii (CR)
Opti = 8.4E-01
G. gorilla (CR)
Opti = 7.08E-01
P. paniscus (EN)
Opti = 5.27E-01
P. troglodytes (EN)
Opti = 5.51E-01
H. sapiens
Opti = 5.79E-01
0.65
0.55
Relative frequency
Observed
Control
PTI score
Strepsirrhini
Tarsier
Platyrrhini
Cercopithecidae
Hylobatidae
Pongo
Gorilla
Hominini
B
O. cuniculus (EN)
Opti = 4.79E-01
C. lanigera (EN)
Opti = 6.95E-01
C. canadensis (LC)
Opti = 5.90E-01
J. jaculus (LC)
Opti = 5.91E-01
N. galili
Opti = 7.16E-01
R. norvegicus (LC)
Opti = 6.82E-01
M. musculus (LC)
Opti = 6.21E-01
observed
control
Lagomorpha
Rodentia
C
M. lucifugus (EN)
Opti = 6.93E-01
F. catus
Opti = 4.01E-01
U. americanus (LC)
Opti = 5.07E-01
C. familiaris
Opti = 3.80E-01
E. asinus
Opti = 4.18E-01
E. caballus
Opti = 3.66E-01
T. truncatus (LC)
Opti = 6.13E-01
P. catodon (VU)
Opti = 5.55E-01
S. scrofa (LC)
Opti = 3.91E-01
O. aries
Opti = 4.75E-01
B. taurus
Opti = 4.90E-01
Chiroptera
Carnivora
Perissodactyla
Cetartiodactyla

Figure 6

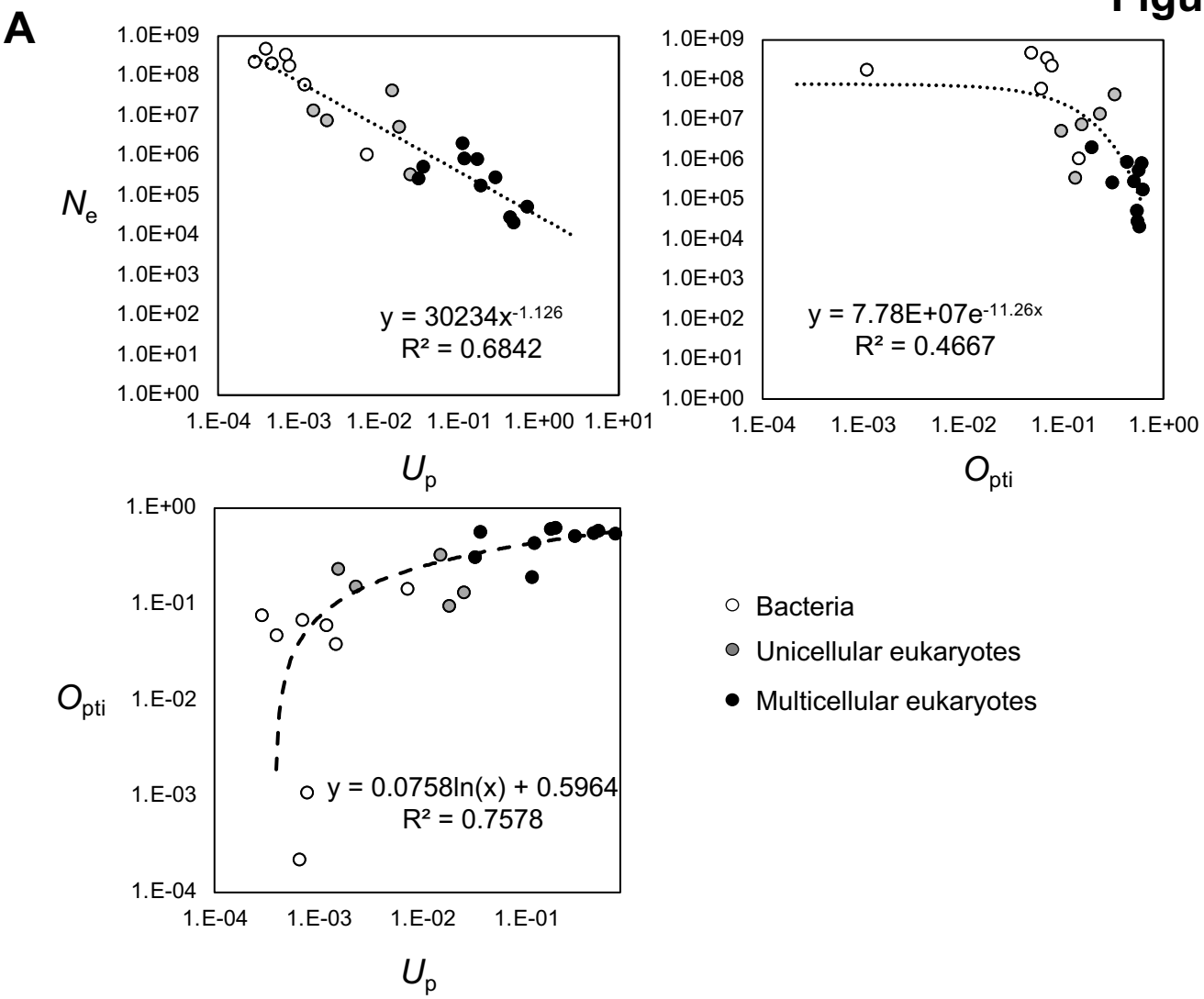
A
N_e
1.0E+09
1.0E+08
1.0E+07
1.0E+06
1.0E+05
1.0E+04
1.0E+03
1.0E+02
1.0E+01
1.0E+00
y = 30234x^-1.126
R² = 0.6842
1.E-04 1.E-03 1.E-02 1.E-01 1.E+00 1.E+01
U_p
y = 7.78E+07e^-11.26x
R² = 0.4667
1.E-04 1.E-03 1.E-02 1.E-01 1.E+00
O_{pti}
1.E+00
1.E-01
1.E-02
1.E-03
1.E-04
y = 0.0758ln(x) + 0.5964
R² = 0.7578
1.E-04 1.E-03 1.E-02 1.E-01
U_p
Bacteria
Unicellular eukaryotes
Multicellular eukaryotes

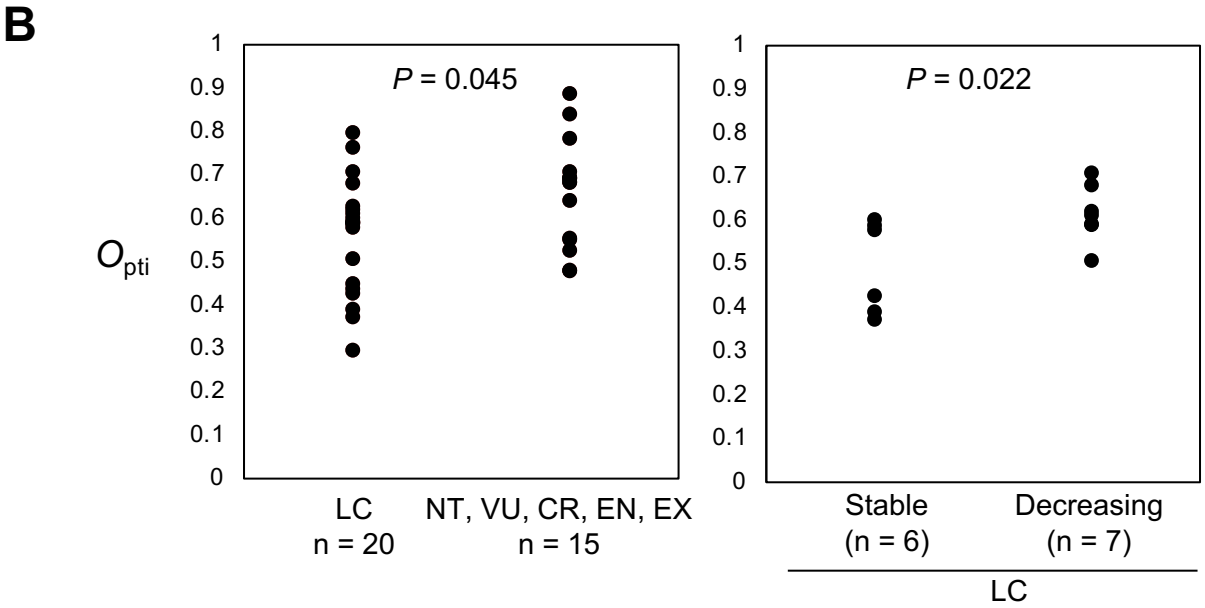
B
O_{pti}
1
0.9
0.8
0.7
0.6
0.5
0.4
0.3
0.2
0.1
0
P = 0.045
LC
n = 20
NT, VU, CR, EN, EX
n = 15
P = 0.022
Stable
(n = 6)
Decreasing
(n = 7)
LC

Figure 7

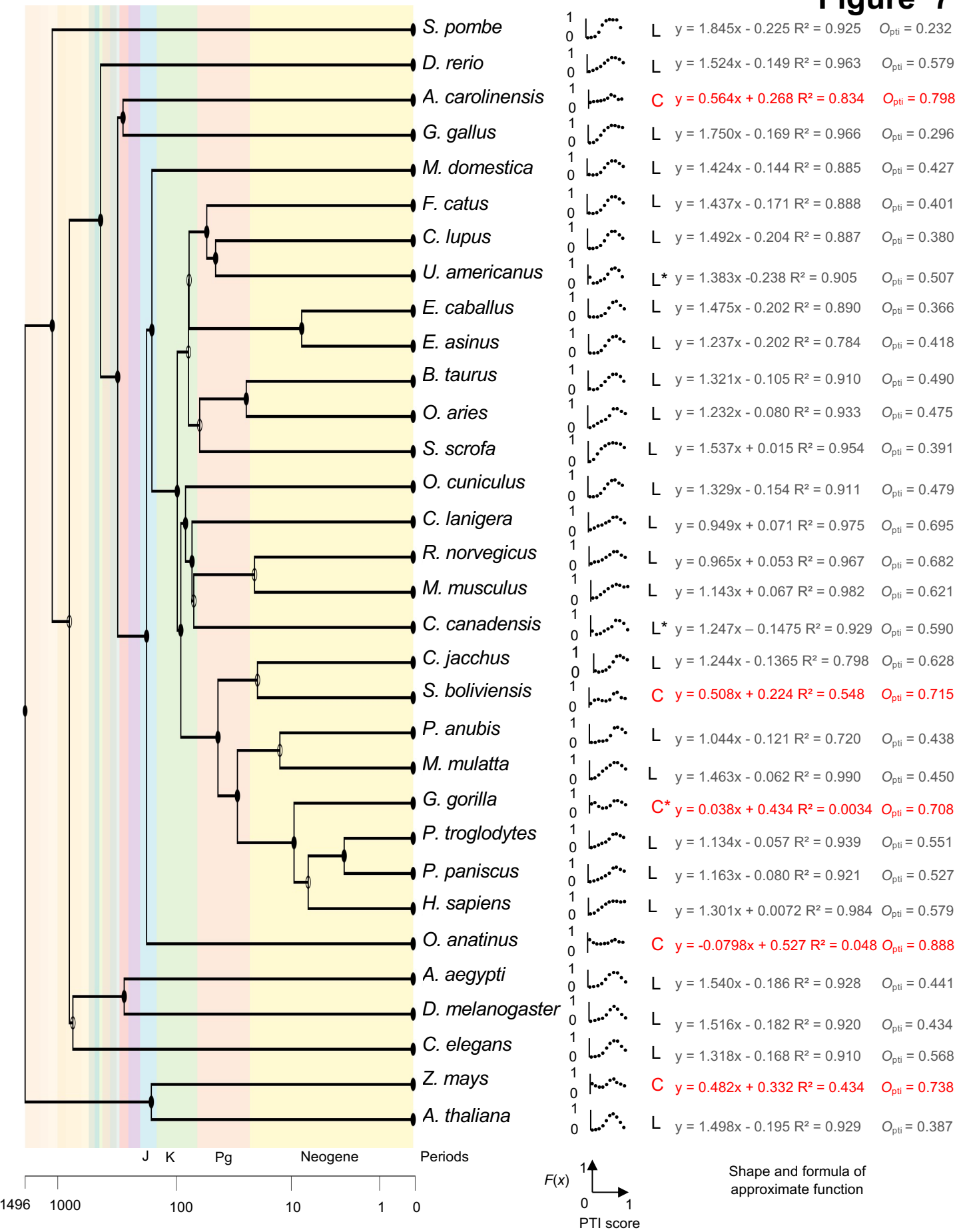
S. pombe
D. rerio
A. carolinensis
G. gallus
M. domestica
F. catus
C. lupus
U. americanus
E. caballus
E. asinus
B. taurus
O. aries
S. scrofa
O. cuniculus
C. lanigera
R. norvegicus
M. musculus
C. canadensis
C. jacchus
S. boliviensis
P. anubis
M. mulatta
G. gorilla
P. troglodytes
P. paniscus
H. sapiens
O. anatinus
A. aegypti
D. melanogaster
C. elegans
Z. mays
A. thaliana
L y = 1.845x - 0.225 R² = 0.925 Opti = 0.232
L y = 1.524x - 0.149 R² = 0.963 Opti = 0.579
C y = 0.564x + 0.268 R² = 0.834 Opti = 0.798
L y = 1.750x - 0.169 R² = 0.966 Opti = 0.296
L y = 1.424x - 0.144 R² = 0.885 Opti = 0.427
L y = 1.437x - 0.171 R² = 0.888 Opti = 0.401
L y = 1.492x - 0.204 R² = 0.887 Opti = 0.380
L* y = 1.383x -0.238 R² = 0.905 Opti = 0.507
L y = 1.475x - 0.202 R² = 0.890 Opti = 0.366
L y = 1.237x - 0.202 R² = 0.784 Opti = 0.418
L y = 1.321x - 0.105 R² = 0.910 Opti = 0.490
L y = 1.232x - 0.080 R² = 0.933 Opti = 0.475
L y = 1.537x + 0.015 R² = 0.954 Opti = 0.391
L y = 1.329x - 0.154 R² = 0.911 Opti = 0.479
L y = 0.949x + 0.071 R² = 0.975 Opti = 0.695
L y = 0.965x + 0.053 R² = 0.967 Opti = 0.682
L y = 1.143x + 0.067 R² = 0.982 Opti = 0.621
L* y = 1.247x – 0.1475 R² = 0.929 Opti = 0.590
L y = 1.244x - 0.1365 R² = 0.798 Opti = 0.628
C y = 0.508x + 0.224 R² = 0.548 Opti = 0.715
L y = 1.044x - 0.121 R² = 0.720 Opti = 0.438
L y = 1.463x - 0.062 R² = 0.990 Opti = 0.450
C* y = 0.038x + 0.434 R² = 0.0034 Opti = 0.708
L y = 1.134x - 0.057 R² = 0.939 Opti = 0.551
L y = 1.163x - 0.080 R² = 0.921 Opti = 0.527
L y = 1.301x + 0.0072 R² = 0.984 Opti = 0.579
C y = -0.0798x + 0.527 R² = 0.048 Opti = 0.888
L y = 1.540x - 0.186 R² = 0.928 Opti = 0.441
L y = 1.516x - 0.182 R² = 0.920 Opti = 0.434
L y = 1.318x - 0.168 R² = 0.910 Opti = 0.568
C y = 0.482x + 0.332 R² = 0.434 Opti = 0.738
L y = 1.498x - 0.195 R² = 0.929 Opti = 0.387
J K Pg Neogene Periods
1496 1000 100 10 1 0
F(x)
PTI score
Shape and formula of approximate function

Figure 8

A

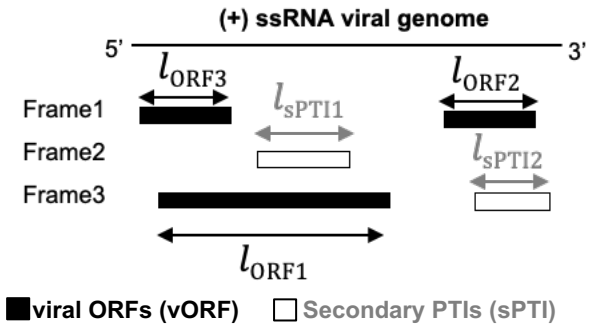

$$\sum l_{vORF} = l_{vORF1} + l_{vORF2} + \cdots + l_{vORFn}$$

$$\sum l_{sPTI} = l_{sPTI1} + l_{sPTI2} + \cdots + l_{sPTIn}$$

$$\text{vORF score} = \frac{\sum l_{vORF}}{\sum l_{vORF} + \sum l_{sPTI}}$$

B

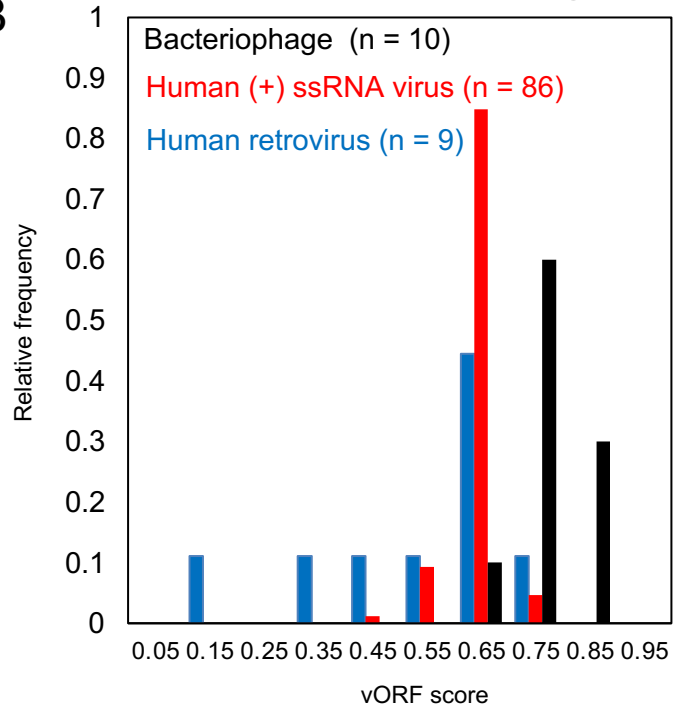

C

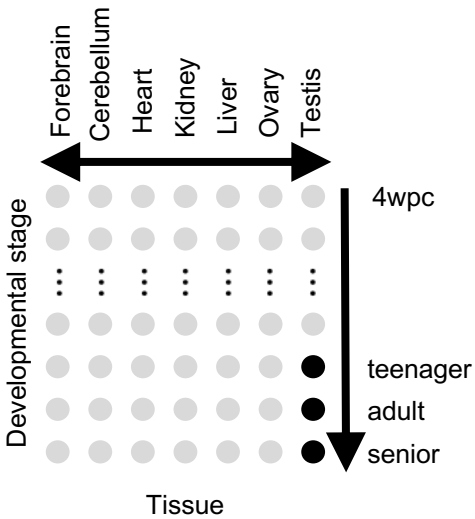

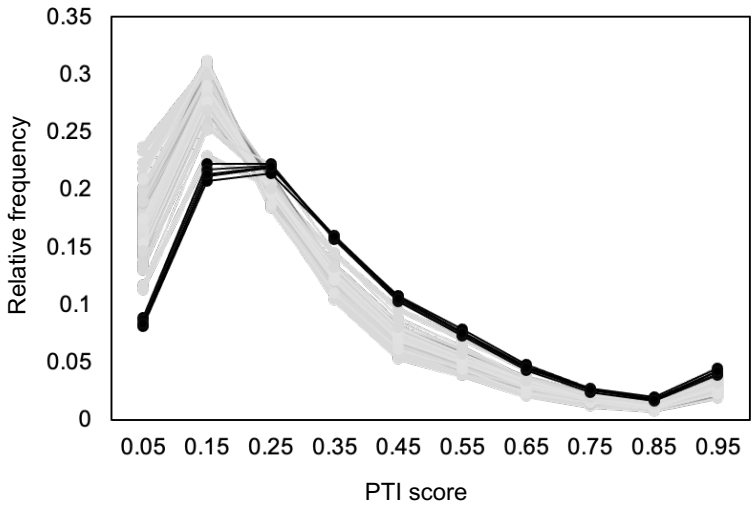

D

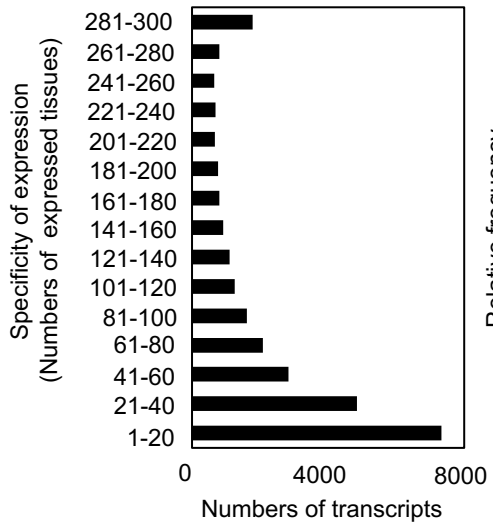

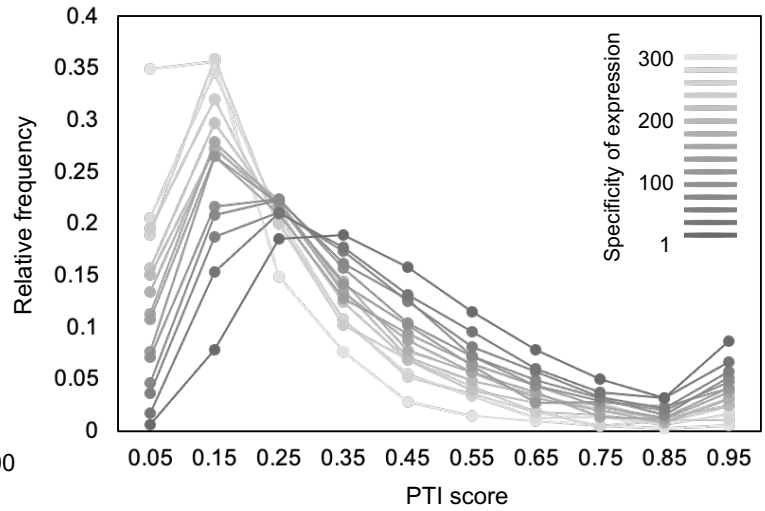

A

Figure 9

Prokaryotes

PTI score
- high → toxicity
  - high → negative selection
  - low → new coding gene
- low → noncoding RNA

Unicellular eukaryotes

PTI score
- high → localization
  - cytosolic → toxicity
    - high → negative selection
    - low → new coding gene
  - nuclear → noncoding RNA
- low → noncoding RNA

Multicellular eukaryotes

expression	probability of toxicity	negative selection	new coding gene
ubiquitous	high	high	rare
specific	low	low	frequent

PTI score
- high → localization
  - cytosolic → expression
  - nuclear → noncoding RNA
- low → noncoding RNA
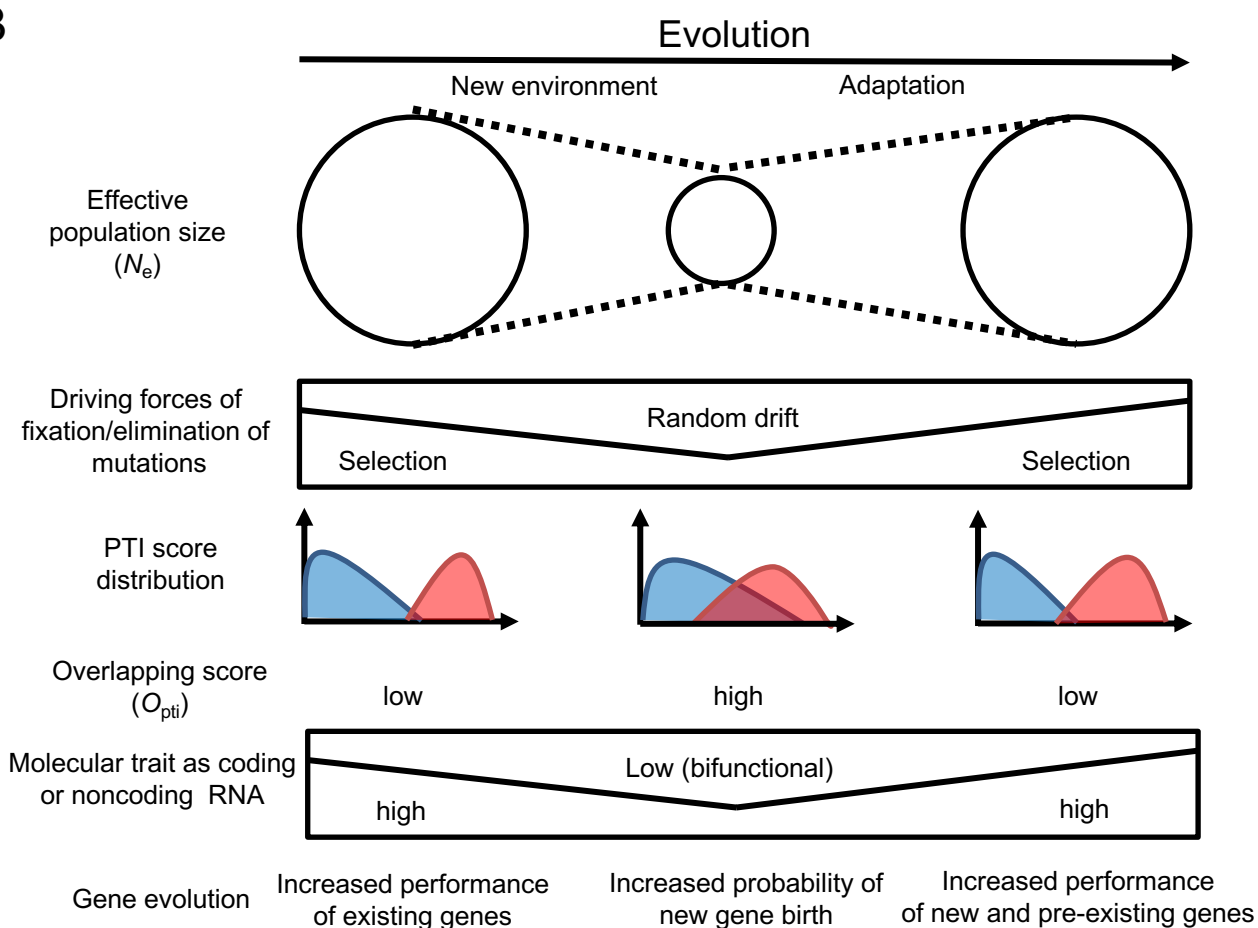
B